Scientific Reports

https://doi.org/10.1038/s41598-026-47473-y

Article in Press

Ameliorative role of apricot shell-derived biochar in modulating photosynthetic pigments, osmolytes, and secondary metabolites in chromium stressed *Brassica juncea*

Received: 16 October 2025

Accepted: 31 March 2026

Published online: 06 May 2026

Cite this article as: Mir N.R., Mavi M.S. & Kapoor N. Ameliorative role of apricot shell-derived biochar in modulating photosynthetic pigments, osmolytes, and secondary metabolites in chromium stressed *Brassica juncea*. *Sci Rep* (2026). https://doi.org/10.1038/s41598-026-47473-y

Nahida Rehman Mir, Manpreet Singh Mavi & Nitika Kapoor

Ameliorative Role of Apricot Shell-Derived Biochar in Modulating Photosynthetic Pigments, Osmolytes, and Secondary Metabolites in Chromium Stressed *Brassica juncea*

Nahida Rehman Mir[1], Manpreet Singh Mavi[2] and Nitika Kapoor[1,*]

[1]Department of Botanical and Environmental Sciences, Guru Nanak Dev University, Amritsar-143005, Punjab (India)

[2]Department of Soil Science, Punjab Agricultural University, Ludhiana-141004, Punjab, (India)

[*]Email of corresponding author: [*]Nitika Kapoor: nitikaarora8@gmail.com

Abstract

Chromium (Cr), a redox-active heavy metal, induces oxidative stress in plants by generating reactive oxygen species (ROS) such as hydrogen peroxide, superoxide anion, and hydroxyl radicals, which reduce plant productivity and yield. This study evaluated the potential of biochar (BC) derived from apricot kernel shells to alleviate Cr toxicity in *Brassica juncea*. The BC was characterized as amorphous, alkaline (pH 7.84), with a zeta potential of –22.3 mV, and elemental composition of C (60.70%), O (29.58%), H (2.65%), and N (0.77%). FTIR analysis revealed multiple oxygen-containing functional groups, suggesting its capacity to reduce Cr mobility. The alkaline nature and porous structure of the BC further support its immobilization potential.

Seeds of *B. juncea* were germinated in soil treated with 0.5 mM and 0.75 mM Cr, with or without 1% BC (10 g/kg soil). Cr exposure significantly reduced photosynthetic pigments, with total chlorophyll declining by 30.8–49.1% and carotenoids by 25.7–50% compared to control, while pheophytin content increased by 13.9–45.3%. Application of BC improved chlorophyll content and reduced pheophytin accumulation. Secondary metabolites and osmolytes were enhanced under BC and stress treatments, with total phenols increased by up to 45% and total carbohydrates by up to 34%. Growth and germination parameters were also negatively affected by Cr, but BC treatment effectively mitigated these effects, improving root and shoot development.

Overall, apricot kernel shell–derived BC alleviated Cr phytotoxicity by reducing metal availability and enhancing plant growth, photosynthetic performance, and metabolic activity. These findings highlight its potential as an eco-friendly and sustainable strategy for mitigating heavy metal stress in plants

Keywords: Apricot, Biochar, Chromium, Plant Physiology, Stress

1.Introduction

In recent times, the decline in agricultural productivity due to diverse environmental stresses has posed a significant challenge for plant scientists, compelling them to develop effective strategies to minimize crop losses (Al-Huqail et al., 2020b). Plant growth and development are highly susceptible to abiotic stresses, which disrupt key morphological, biochemical, and physiological processes. From germination to maturity, such stresses including heavy metals, extreme temperatures, salinity, drought and waterlogging pose serious constraints on plant performance, ultimately reducing growth and yield (Akram et al., 2020; Al-Huqail et al., 2020a, 2020b). Recently, Cr has emerged as a critical environmental contaminant, driven largely by unsustainable agricultural practices, uncontrolled industrial effluent discharge, and the extensive use of biosolids, posing serious ecological and agricultural threats (Devi et al., 2024). Chromium exists in multiple forms in soil, with hexavalent (Cr(VI)) and trivalent (Cr(III)) species being the most stable and prevalent (Srivastava et al., 2021). Owing to its higher water solubility, Cr becomes more bioavailable to plants (Gupta et al., 2020). Among its oxidation states, Cr(VI) is particularly hazardous, as it readily penetrates plant roots and induces oxidative damage to vital cellular structures (Askari et al., 2021; Kushwaha et al., 2020). Even at trace levels, Cr(VI) can disrupt nutrient and water uptake, leading to nutrient deficiencies in shoots (Bashir et al., 2020). Oxidative damage to root tissues further enhances passive entry of Cr(VI), allowing its translocation to shoots, where it impairs the mitochondrial and photosynthetic systems. Being a strong oxidant, Cr(VI) disrupts photophosphorylation, induces lipid peroxidation, and triggers excessive generation of ROS (Sajad et al., 2020). Due to its structural similarity to sulfate (SO_4^{2-}), CrO_4^{2-} is readily transported into cells *via* sulfate transporters (Ksheminska et al., 2005), where it reacts with antioxidants such as ascorbate (ASA) and glutathione (GSH), generating harmful free radicals. The resulting ROS including singlet oxygen, superoxide, hydroxyl radicals (•OH), and hydrogen peroxide (H_2O_2) (Qamer et al., 2021) can damage DNA–protein complexes, leading to genotoxicity and cytotoxicity (Shanker, 2019). Such adverse effects of Cr(VI) exposure have been widely reported in plants like rice, bush bean, mung bean, mustard, spinach and tomato (Devi et al., 2024; Wakeel et al., 2020; Sehrish et al., 2019). Hence, the challenge of Cr contamination, which hampers agricultural productivity worldwide, has drawn considerable scientific attention.

Several conventional techniques, including ion exchange, membrane filtration, precipitation and coagulation have been employed for the removal of Cr from wastewater (Peng and Guo, 2020). However, their large-scale application is often limited due to inconsistent results and the high operational costs associated with these processes (Peng and Guo, 2020; Ai et al., 2018). Recently, there has been growing interest in using low-cost materials as adsorbents (Turan et al., 2018). One such material is BC which is a carbon-rich pyrogenic material produced by the thermal decomposition of organic matter in an oxygen-limited environment (Ali et al., 2018). It is primarily derived from feedstocks such as agricultural residues, animal waste, and woody biomass (Rizwan et al., 2018, 2016). Also, by enhancing various key properties of soil, such as its water-holding capacity, organic matter content, cation exchange capacity, pH and microbial activity BC functions as an effective soil conditioner (Wei et al., 2019; Rizwan et al., 2018). Owing to its abundant functional groups, minerals, π-electrons, porous structure and organic matter content, BC regulates Cr bioavailability and stability in soil through multiple mechanisms such as electrostatic interactions, cation exchange, precipitation and complexation (Haider et al., 2022; Wang et al., 2021). Notably, oxygen-containing functional groups, including hydroxyl, carboxyl, and phenolic groups on the BC surface, can effectively bind with soil pollutants (Azeem et al., 2022). Furthermore, the large surface area, high porosity, and well-organized carbon framework of BC (Tomczyk et al., 2020) enable it to act as a potent sorbent for pollutants *via* complexation (Ambaye et al., 2021). This is facilitated by the presence of acidic functional groups (carboxylic, carbonyl, lactone, hydroxyl, and phenol) and basic functional groups (ketone and chromene) (Choppala et al., 2016). Additionally, BC can promote the precipitation of Cr by interacting with soil minerals such as carbonates, oxides, and phosphates (Al-Wabel et al., 2015; Lu et al., 2012). Prior studies have also highlighted the ability of BC active sites, such as carboxylic acid (−COOH), carbonyl (−C=O), and inorganic ions (e.g., PO□³□), to bind toxic metals, thereby reducing their mobility in soil (Liang et al., 2021; Duwiejuah et al., 2020). Collectively, these attributes underscore BC effectiveness as both an environmental adsorbent and a stabilizing agent for organic and inorganic soil contaminants (Ai et al., 2018). Moreover, BC possesses the ability to reduce Cr(VI) to its less toxic trivalent form, Cr(III), further mitigating its environmental hazards (Mandal et al., 2017). In addition to these mechanisms, several studies have demonstrated the practical effectiveness of BC in contaminated soils. For example, bamboo BC application in mine-polluted soils improved soil physicochemical properties and reduced the bioavailability and uptake of toxic metals, thereby

enhancing antioxidant defense and biomass accumulation in *Brassica juncea* (Emamverdian et al., 2024). Similarly, kenaf BC effectively mitigated HM stress and enhanced phytoremediation in *Cannabis sativa*. The BC exhibited strong chemisorption capacity in a multi-metal system, particularly for Cd^{2+} and Zn^{2+}, which significantly reduced their bioavailability in soil (Pan et al., 2025). The application of BC prepared from eucalyptus n bamboo (*Sasa kongosanensis* f. *aureo-striatus*) under copper stress enhanced the plant defense system by stimulating antioxidant enzymes such as superoxide dismutase (SOD), catalase (CAT), peroxidase (POD), and phenylalanine ammonia-lyase (PAL), along with improving the efficiency of the glyoxalase detoxification pathway. It also promoted the accumulation of osmolytes, particularly proline and glycine betaine, which contributed to osmotic balance and protection against oxidative stress. Consequently, oxidative damage was alleviated. Furthermore, the treatments improved photosynthetic pigment content, gas-exchange attributes, and plant water status, while simultaneously reducing copper translocation and bioaccumulation in plant tissues (Emamverdian et al., 2025). Another, popular ameliorator among researchers is nanoparticles, they help plants in scavenging excessive ROS induced by heavy metal (HM) stress by increasing the activity of antioxidative enzymes and can reduce the accumulation and uptake of HMs (Emamverdian et al., 2025; Huang et al., 2025). Nanoparticles mainly act inside plants however BC immobilizes HM in soil, thereby reducing their bioavailability before plant uptake (Shah and Aslam, 2025; Ghandali et al., 2024; Gong et al., 2022). Biochar being aromatic in nature is highly stable and remain effective for hundreds or thousands of years but nanoparticles may transform, dissolve, or leach, reducing long-term effectiveness (Irumva et al., 2025; Schmidt et al., 2022). Considering the documented benefits of BC in regulating Cr bioavailability and stability in soil, as well as enhancing plant growth and development under Cr stress, we propose using apricot shell-derived BC to mitigate Cr toxicity in *Brassica juncea* L. seedlings which was assessed by evaluating various growth and biochemical parameters. Based on this, the present study was designed with the following objectives:

- To prepare and characterize BC from the apricot kernel shells.
- To investigate the effect of BC on the growth parameters of Cr-stressed *Brassica juncea* L.
- To investigate the effect of BC on the physiological parameters of Cr-stressed *Brassica juncea* L.

2. Materials and Methods

2.1. Biochar Preparation Process

The raw material used for the preparation of BC was apricot (*Prunus armeniaca* L.) kernel shells, procured from the Kargil district of UT Ladakh. The apricot shells were washed with distilled water and allowed to dry naturally. The dried shells were then pyrolyzed in a single-screw pyrolysis reactor at a temperature of 500-550°C for 3-4 minutes (residence time). The black residue (BC) obtained after pyrolysis was allowed to cool, finely ground, and subsequently passed through a 0.5 mm mesh before application (Figure 1).

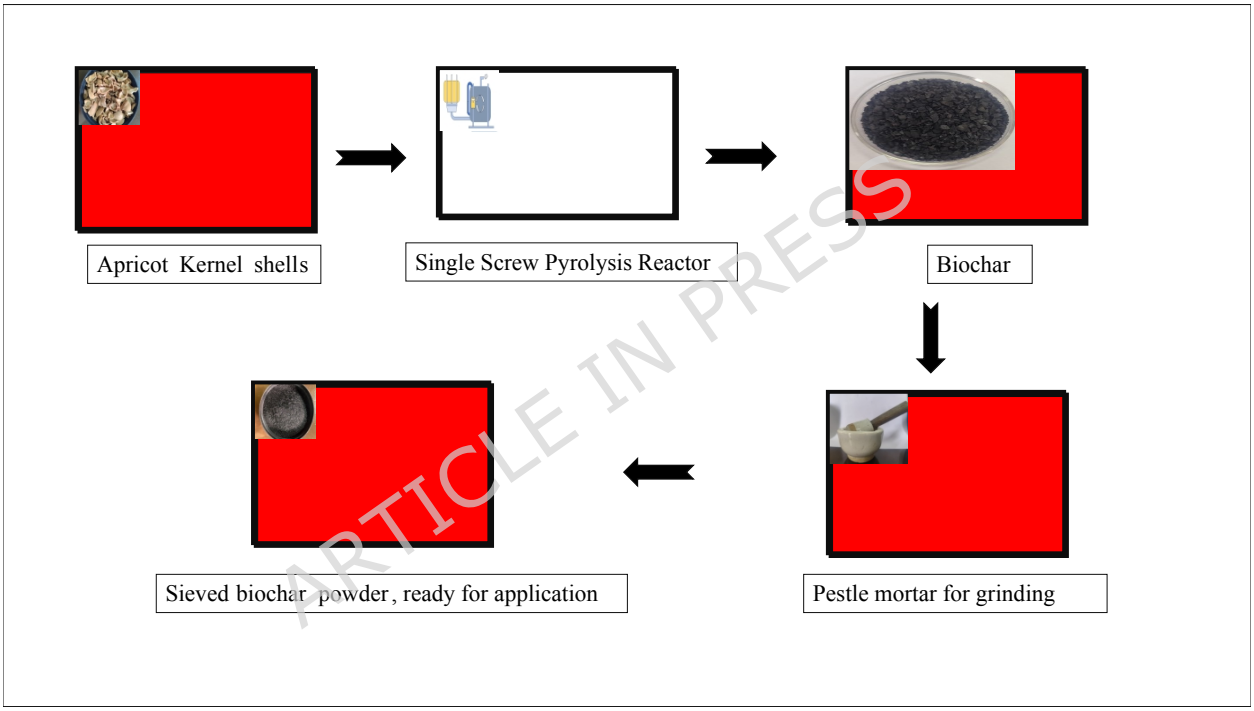

Figure 1: Preparation of biochar from the Apricot Kernel shells

2.2. Characterization of Biochar

The percentage yield of BC after pyrolysis was calculated as the ratio of the produced BC mass to the initial biomass, (Yield (%) = Weight of BC / weight of biomass × 100) (Sahoo et al., 2021) which was 40%.

For proximate analysis, 1g BC was combusted for 2 hrs at 800°C ± 20°C, and the residual mass percentage was determined as the ash content. Fixed carbon content was estimated by calculating

the difference between the BC total dry weight and the combined proportions of ash and volatile matter. The volatile matter content was measured by recording the mass loss of a 1.0 g BC sample after combustion in a muffle furnace at 850°C for 1 minute. The oven dried (80°C) and finely powdered BC samples were further analyzed using elemental analyzer (Thermo Scientific, Flash 2000) to estimate the percentage of C, H, N. The amount of oxygen in the sample was calculated by subtracting total percentage of carbon, nitrogen, hydrogen, sulphur and ash from 100 (Castan et al., 2019).

Fourier-transform infrared (FTIR) spectroscopy analysis was conducted on the apricot kernel shell BC sample produced at 500°C. The spectra of FTIR were obtained using Shimadzu-FTIR and then the measurements were performed on the dry powdered samples. High-quality spectral lines, were recorded between 4000 and 400 cm^{-1} and to estimate the surface area, pore volume and diameter, Brunauer-Emmett-Teller (BET) surface analyzer was used. Furthermore, SEM-EDS was also conducted to characterize the surface morphology and elemental composition of the prepared BC.

2.3. Experimental design

The experiment was conducted under *in-vitro* conditions at 25 ± 2°C with a 16-hours photoperiod. A total of six treatments, each with three replicates were included: Control, M1, M2, BC, BC+M1 and BC+M2 (Table 1). HM stress was induced using potassium chromate (K_2CrO_4) as a source of hexavalent chromium [Cr(VI)]. The Cr concentrations used in this study were selected based on IC_{50} (0.5 mM) and IC_{75} (0.75 mM) values (**supplementary material, Table S1; Figure S1**), which were determined from preliminary toxicity experiments by evaluating the inhibition of root elongation in seedlings exposed to different Cr concentrations. Biochar was applied at a rate of 1% (10 g kg^{-1} soil), on the bases of preliminary trials against 0.5 mM Cr in which this concentration was found to be effective in alleviating Cr-induced toxicity, particularly in terms of root length reduction in *Brassica juncea* L. seedlings.

Brassica juncea L. seeds, obtained from Punjab Agricultural University, Ludhiana, Punjab, India, were surface-sterilized with 0.24% sodium hypochlorite prior to sowing. Seedlings were harvested after 10 days, thoroughly rinsed with distilled water, and processed for further analyses.

Table 1: Various Treatments and their concentration used in the study

S.NO.	Treatments	Biochar	Cr VI
1.	Control	0	0
2.	M1	0	0.5mM
3.	M2	0	0.75mM
4.	BC	1%	0
5.	BC+M1	1%	0.5mM
6.	BC+M2	1%	0.75mM

2.4. Growth Analysis

At the end of each harvest, the seedlings were uprooted, cleansed with tap water to remove residual debris, and finally rinsed with distilled water. Subsequently, various parameters were analyzed.

2.4.1. Fresh Weight, Dry Weight and Moisture content

The fresh weights (g) of the seedlings were determined using a digital balance in the laboratory, while the method proposed by Wolf et al. (1997) was followed to determine dry weight and moisture content of the seedling. The weight of an empty evaporating dish was recorded, after which fresh plant material was added and the combined weight was noted. The dish containing the sample was then oven-dried at 102–105 °C for 16 hours. Once dried, the dry weight of the seedlings was measured. The recorded fresh and dry weights were subsequently used to calculate the moisture content of the seedlings using the following formula:

$$\text{Moisture Content (\%)} = \frac{(\text{weight of wet sample + evap. dish}) - (\text{weight of dry sample + evap. dish})}{(\text{weight of wet sample + evap. dish}) - (\text{weight of empty evap. dish})} \times 100$$

2.4.2. Root Length and Shoot Length

At the time of harvest, shoot and root lengths (cm) were measured using a centimeter scale.

2.4.3. Stress Tolerance Index

Various stress tolerance indices were determined to assess plant performance under stress conditions. These included the shoot height stress tolerance index (SHSTI), root length stress

tolerance index (RLSTI), and stress tolerance indices for total fresh weight (FWSTI) and dry weight (DWSTI), which were computed using the respective formulas provided by Abdelhameed and Metwally, (2025).

$$\text{DWSTI}(\%) = \frac{\text{Dry weight of treated plants}}{\text{Dry weight of untreated plants}} \times 100$$

$$\text{FWSTI}(\%) = \frac{\text{Fresh weight of treated plants}}{\text{Fresh weight of untreated plants}} \times 100$$

$$\text{SHSTI}(\%) = \frac{\text{Shoot height of treated plants}}{\text{Shoot height of untreated plants}} \times 100$$

$$\text{RLSTI}(\%) = \frac{\text{Root length of treated plants}}{\text{Root length of untreated plants}} \times 100$$

2.4.4. Germination Percentage

The germination percentage was estimated using the Close & Wilson (2002) method.

$$\text{Germination percentage} = \frac{\text{Number of seeds germinated}}{\text{Total no. of seeds sown}} \times 100$$

2.4.5. Seedling vigor index

Seedling vigor index for seedling height was calculated using Bina and Bostani, (2017) standard formula. The length of the seedlings in centimeters was multiplied by the germination % to calculate the Seedling vigor index

Seedling vigor index = seedling length (cm) × seed germination percentage

2.4.6. Germination Mean Time

The formula proposed by Ellis and Roberts (1981) was used to calculate the germination mean time.

$$\text{Germination Mean Time} = \frac{\sum(ni \times ti)}{\sum ni}$$

Where,

ni = no. of seeds germinated on day i.

ti = time in days from the start of experiment to day i

∑ni = Total no. of seeds germinated over the entire period **2.5. Photosynthetic Pigments Content**

2.5.1. Chlorophyll Content

The methodology proposed by Lichtenthaler (1987) was followed for the estimation of chlorophyll content. Fresh plant tissue about 1g was homogenized in acetone (80%) using a chilled mortar and pestle to preserve pigment integrity. The resulting homogenate was then subjected to centrifugation at 4°C for 20 minutes at 13,000 rpm (or ≈ 11,336 × *g*). Following centrifugation, the clear supernatant was carefully collected and its absorbance was recorded at wavelengths of 647 nm and 663 nm using a UV-Vis spectrophotometer.

2.5.2. Total Carotenoid

Methodology of Maclachlan and Zalik (1963) was followed to determine the Total carotenoid content. 1g of fresh plant material was finely ground with 80% acetone in a pre-chilled mortar and pestle to ensure effective pigment extraction. The homogenized mixture was then centrifuged at 13,000 × g for 20 minutes at 4°C. After centrifugation, the clear supernatant was collected, and its absorbance was measured at 480 nm and 510 nm using a UV-Visible spectrophotometer to analyze pigment content.

2.5.3. Pheophytin Content

The methodology proposed by Lichtenthaler (1987) was followed for the estimation of pheophytin content. Briefly, fresh plant material (1 gram) was thoroughly ground in a chilled mortar and pestle using 80% acetone as the extraction solvent. The homogenate was centrifuged at 5,000 rpm (or ≈ 1,677 × *g*) for 15 minutes at 4°C. After centrifugation, the supernatant was carefully collected and 25% HCl was added to it. The absorbance of the final reaction mixture was then measured at 653 nm and 665 nm to assess pigment content.

2.6. Secondary Metabolites

2.6.1. Phenol content

The procedure outlined by Singleton and Rossi, (1965) was followed for the analysis of the total phenol content in the seedlings of *Brassica juncea.* Around 0.5 grams of the dry sample was pulverized using 60% ethanol and kept in a water bath (65°C) for 10-15 minutes. The homogenate was filtered using whatman no.1 filter paper and then the volume was raised to 100 ml by adding 60% ethanol followed by mixing 2ml of the mixture with Folin-Ciocalteu reagent and sodium carbonate. The resulting mixture was then incubated for 2 hours and the optical density was noted at 765 nm.

2.6.2. Anthocyanin Content

To determine the anthocyanin content, 1 gram of the fresh seedlings were subjected to crushing in 3 ml of acidified methanol by following the methodology of Mancinelli, (1990). The homogenate was then centrifuged for 25 minutes at 12000 rpm (or ≈ 9,659 × *g*) followed by recording the absorbance at 530 nm and 657 nm.

2.6.3. Flavonoid content

By following the methodology of El Far and Taie, (2009) total flavonoid content was estimated. Briefly, 100 mg of sample was crushed with the help of mortar and pestle using 4 ml of absolute methanol, after which the homogenate was centrifuged (13000 rpm or ≈ 11,336 × *g*, 4°C, 20 minutes). The supernatant (1.5 ml) was mixed with equal volume of 2% $AlCl_3$ (2 g in 100 ml methanol). The resulting solution was shaken vigorously and incubated for 10 minutes followed by measuring the absorbance at 367 nm.

2.7. Osmolyte

2.7.1. Total Carbohydrate

To estimate the content of total carbohydrate 0.1 gram of oven dried sample was immersed in 5 ml of 2.5N HCl for 3 hours in a boiling water bath by following the methodology of Hedge, (1962). The sample was then cooled, neutralized using Na_2CO_3 and volume was raised to 100 ml followed by centrifugation. To 1 ml of the sample 4 ml of the anthrone reagent was added and the solution

was again heated for 8 minutes after which the samples were cooled and absorbance was recorded at 630 nm.

2.7.2. Trehalose

The methodology of Trevelyn and Harrison, (1956) was followed to analyze the content of trehalose in the seedlings of *Brassica juncea*. 500 mg of the dried sample was homogenized in 80% ethanol. The resulting homogenate was subjected to centrifugation for 10 minutes at 5000 rpm (or ≈ 1,677 × *g*), 4°C. To the supernatant (0.1 ml), 2 ml of trichloroacetic acid and 4 ml of anthrone was added after which absorbance was recorded at 620 nm.

2.7.3. Proline

The methodology of Bates et al. (1973) was used for the estimation of proline content spectrophotometrically at 520 nm. 500 mg of fresh seedlings were homogenized using 3% sulfosalicylic acid and then the homogenate was centrifuged (12 min and 13,000 rpm or ≈ 11,336 × *g*). To the supernatant an equal volume of ninhydrin and glacial acetic acid was added the reaction mixture was then heated at 95 ± 5 °C. After 1 hour the reaction was terminated by placing the test tubes in ice-bath followed by the incorporation of toluene.

2.8. Statistical Analysis

The data were statistically analyzed using IBM SPSS statistics version 25 software. All experiments were performed in triplicate, and results are presented as mean ± standard deviation. One-way analysis of variance (ANOVA) was used to determine significant differences among treatments, followed by Tukey's multiple comparison test for mean separation. Statistical significance was considered at $p \leq 0.05$.

3. Results

3.1. Characterization of Biochar

Various physical and chemical properties of BC were analyzed using standard protocols. The BC prepared from apricot kernel shell at a pyrolysis temperature of 500–550 °C exhibited a pH of 7.84, EC of 0.223 dS/m, 0.563% N, H/C ratio of 0.442, and O/C ratio of 0.192. It also contained 6.3% ash and 9.27% volatile matter (Table 2). The observed physicochemical characteristics are strongly influenced by the applied pyrolysis temperature. At 500–550 °C, substantial thermal

degradation of labile components such as hemicellulose and cellulose occurs, leading to increased carbonization, reduced volatile matter, and enrichment of mineral ash content. This explains the relatively low volatile matter and moderate ash content, along with the slightly alkaline pH due to the accumulation of basic mineral constituents.

The elemental composition, particularly the low H/C (0.442) and O/C (0.192) ratios, indicates an increased degree of aromaticity and structural stability, which is characteristic of BC produced at intermediate to high temperatures. These ratios suggest the formation of condensed aromatic carbon structures through dehydration and decarboxylation reactions during pyrolysis, enhancing the recalcitrance and persistence of BC in soil systems.

Fourier-transform infrared spectroscopy (FTIR) analysis revealed that the BC displayed a variety of absorption bands at different wavelengths. The FTIR spectrum (Figure 2) showed characteristic peaks corresponding to key functional groups. The broad band at 3418 cm^{-1} corresponded to O–H stretching (Zhang et al., 2022), while peaks at 2923 and 2852 cm^{-1} were attributed to –CH$_2$ and –CH$_2$– groups of long-chain saturated alkanes (Zhang et al., 2022). A distinct absorption at 1733 cm^{-1} represented C=O stretching of carbonyl groups (Younis et al., 2017). The bands at 1462 and 1377 cm^{-1} were linked to C=C vibrations of aromatic rings and C–H bending of alkyl groups, respectively (Zahra et al., 2024). Additionally, the peak at 1417 cm^{-1} indicated O–H bending vibrations of alcohols (Hussain et al., 2025), and the band at 978 cm^{-1} corresponded to C=C vibrations of alkenes (Hussain et al., 2025). These functional groups suggest that, despite pyrolysis at 500–550 °C, a fraction of oxygen-containing groups is retained, which can play a crucial role in metal adsorption through surface complexation and electrostatic interactions.

Figure 3 represents the X-ray diffraction (XRD) pattern of apricot kernel shell-derived BC. The results show no sharp crystalline peaks; however, diffraction peaks at $2\theta = 9.8°$ and 22.7° are attributed to the (002) planes of amorphous carbon, indicating a disordered structure (Mokubung et al., 2024; Masuku et al., 2024). A minor peak at $2\theta = 43.0°$ corresponds to the (100) plane of graphitic carbon, suggesting the presence of a small fraction of graphitized domains. This partial structural ordering is consistent with pyrolysis in the 500–550 °C range, where complete graphitization does not occur but initial development of graphitic structures begins.

Furthermore, the FESEM micrographs (Figure 4 and Table 3) show a heterogeneous and porous structure, which is a characteristic outcome of pyrolysis at this temperature range. The irregular

surface morphology and well-developed pore networks are formed due to the release of volatile compounds during thermal decomposition. The formation of such pores enhances the surface heterogeneity and provides active sites for adsorption processes.

Surface area analysis further indicated a pore volume of 0.004 cm^3/g, a Brunauer–Emmett–Teller (BET) surface area of 1.387 m^2/g, and an average pore diameter of 1.8 nm, suggesting the presence of predominantly microporous structures. Although higher pyrolysis temperatures generally increase surface area, the relatively low BET value observed here may be due to pore blockage or collapse caused by tar deposition during pyrolysis. Nevertheless, the developed porosity, as confirmed by FESEM, is sufficient to support adsorption and immobilization processes.

The zeta potential of −22.3 mV indicates a negatively charged surface, which can be attributed to the presence of residual oxygen-containing functional groups. This negative surface charge enhances the electrostatic attraction of positively charged metal ions, thereby improving the adsorption capacity of BC.

Overall, the pyrolysis temperature of 500–550 °C resulted in BC with a balanced combination of aromatic stability, residual functional groups, and porous structure. These characteristics are particularly advantageous for environmental applications, especially in the immobilization of heavy metals, as they provide both structural stability and reactive surface sites.

Table 2: Physicochemical Characteristics of Biochar

S.NO.	Physicochemical Characteristics	Units	BC
1.	**pH (1:25)**	**-**	7.84
2.	**EC (1:25)**	**dS/m**	0.223
3.	**Volatile matter**	**%**	9.27
4.	**Ash Content**	**%**	6.3
5.	**Total Carbon**	**%**	60.703
6.	**Hydrogen**	**%**	2.649
7.	**Oxygen**	**%**	29.582
8.	**Nitrogen**	**%**	0.766
9.	**H/C**	**-**	0.442
10.	**O/C**	**-**	0.192

11.	**Surface area**	m^2/g	1.387□
12.	**Pore volume**	cm^3/g	0.004□
13.	**Pore diameter**	nm	1.8□
14.	**Zeta potential**	mV	-22.3

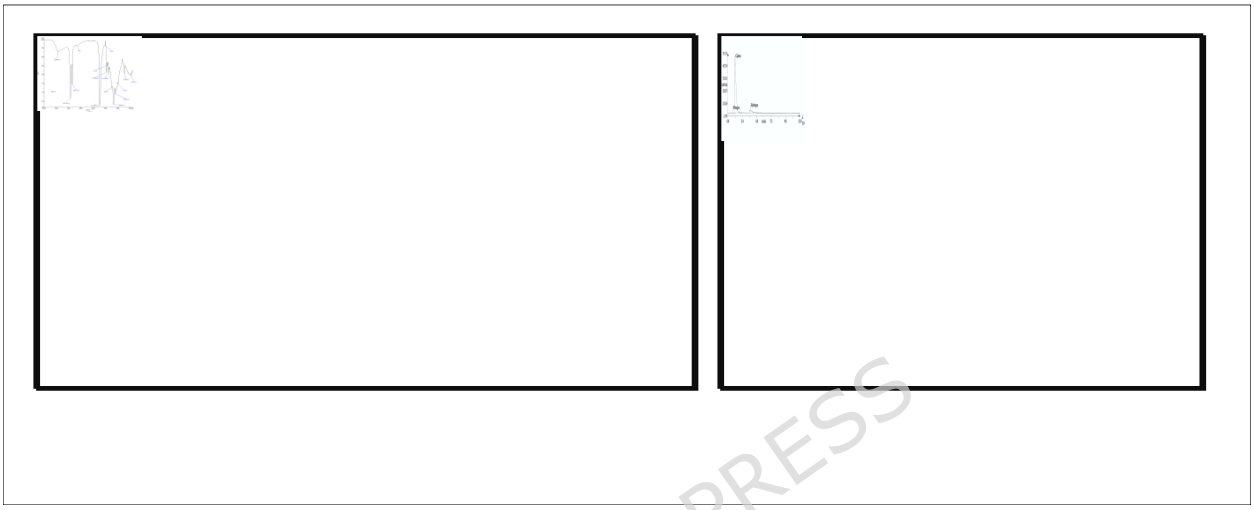

Figure 2: FTIR and CHN spectra of biochar

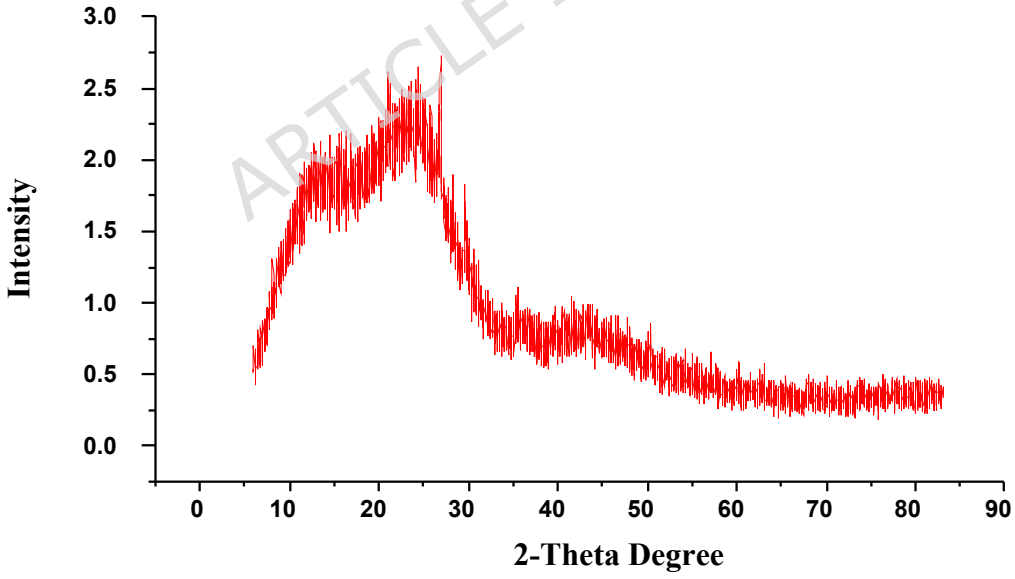

Figure 3: XRD spectra of apricot shell-derived biochar

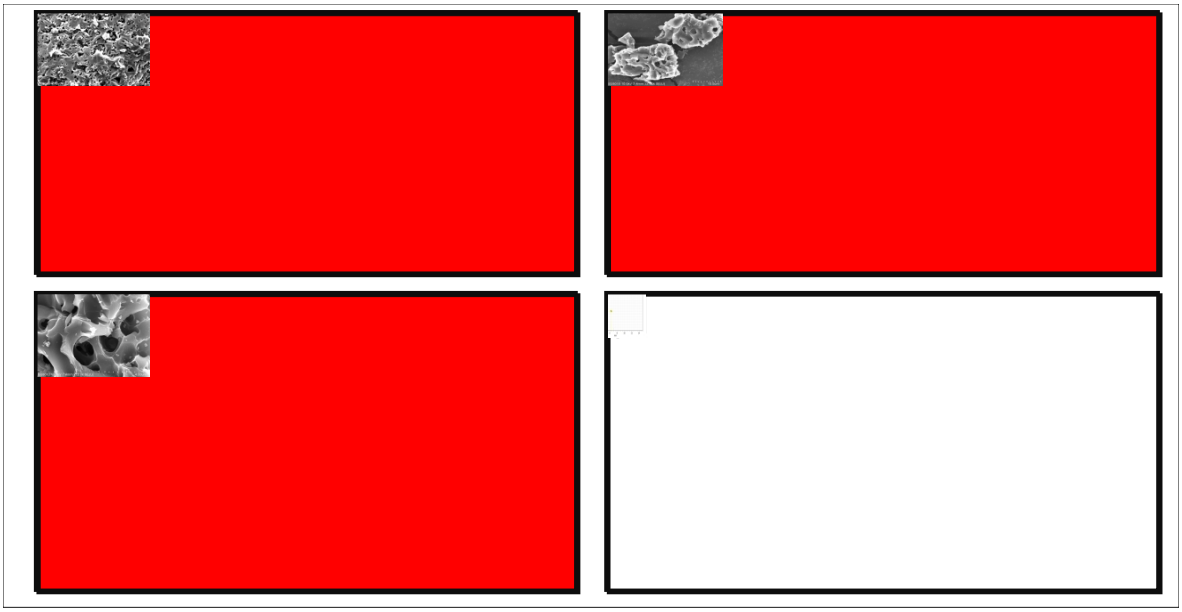

Figure 4: FESEM-EDS images of apricot shell-derived biochar

Table 3: Elemental composition of apricot shell-derived biochar from Energy -dispersive X-ray spectroscopy (EDS)

Biochar	Composition						
	Carbon (%)	Oxygen (%)	Potassium (%)	Calcium (%)	Zirconium (%)	Iron (%)	Silicon (%)
	75.99	16.72	2.69	0.68	1.04	2.01	0.87

3.2. Influence of Biochar on Growth Attributes of *Brassica juncea* Seedlings under Cr Stress

Biochar application significantly improved all growth attributes of Cr-stressed *Brassica juncea* seedlings ($p \leq 0.05$; Figure 5a, b). The most pronounced effect was observed in the BC alone treatment, which showed a significant increase in root length (24.75%), shoot length (35.91%), fresh weight (57.12%), and dry weight (133.3%) compared with the Control. In contrast, Cr only treatments (M1 and M2) exhibited a significant reduction in all growth parameters, with M2 showing significantly lower values than the Control, indicating severe phytotoxic effects. However, the combined application of BC with Cr significantly alleviated this toxicity, as BC+M1 and BC+M2 showed significantly higher growth compared to their respective Cr-only treatments. Notably, BC+M1 was statistically at par with the Control for several growth parameters, indicating

effective mitigation under moderate stress, whereas BC+M2, although significantly improved over M2, remained lower than the Control. A similar trend was observed for moisture content, which decreased under Cr stress but significantly improved upon BC application. Furthermore, the stress tolerance indices, including SHSTI, RLSTI, FWSTI, and DWSTI, were significantly higher in BC-amended treatments compared to Cr-only treatments, confirming the protective role of BC in reducing Cr-induced phytotoxicity and improving overall plant performance. (Table 4).

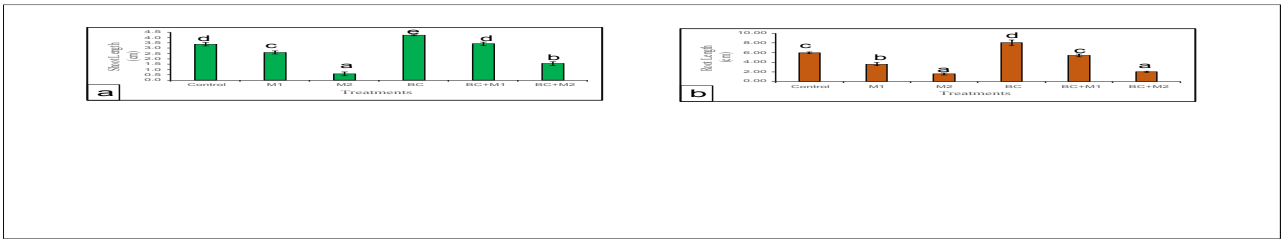

Figure 5a: Effect of Biochar (BC) on (**a**) Shoot Length (**b**) Root length in 10 days old *Brassica juncea* seedlings under chromium (M1 and M2) stress. Bars represent mean ± standard error of three replicates. Different letters above the bars indicate statistically significant differences among treatments according to Tukey's HSD test at $p < 0.05$; bars sharing the same letter are not significantly different.

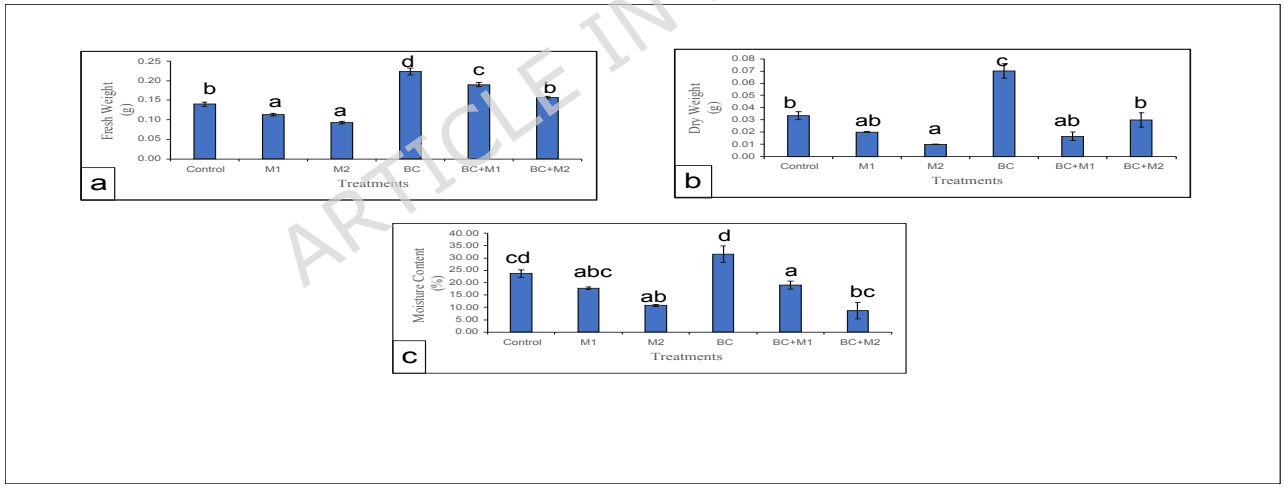

Figure 5b: Effect of Biochar (BC) on (**a**) Fresh Weight (**b**) Dry Weight (**c**) Moisture Content in 10 days old *Brassica juncea* seedlings under chromium (M1 and M2) stress. Bars represent mean ± standard error of three replicates. Different letters above the bars indicate statistically significant differences among treatments according to Tukey's HSD test at $p < 0.05$; bars sharing the same letter are not significantly different.

Table 4: Effect of various treatments on the dry weight stress tolerance index (DWSTI), fresh weight stress tolerance index (FWSTI), shoot height stress tolerance index (SHSTI), and root length stress tolerance index (RLSTI) of *Brassica juncea* seedlings. Values are presented as mean ± standard error of three replicates. Different letters indicate statistically significant differences among treatments according to Tukey's HSD test at $p < 0.05$; values sharing the same letter are not significantly different.

Treatments	DWSTI (%)	FWSTI (%)	SHSTI (%)	RLSTI (%)
Control	-	-	-	-
M1	61.11 ± 5.56^{b}	81.40 ± 5.66^{ab}	61.07 ± 3.67^{b}	77.34 ± 3.33^{c}
M2	30.56 ± 2.78^{a}	67.07 ± 5.08^{a}	26.26 ± 2.49^{a}	18.13 ± 3.76^{a}
BC	-	-	-	-
BC+M1	63.00 ± 3.66^{b}	136.34 ± 8.22^{cd}	91.53 ± 4.01^{c}	101.84 ± 5.45^{cd}
BC+M2	96.00 ± 4^{c}	112.11 ± 2.74^{bc}	33.82 ± 2.03^{ab}	46.02 ± 3.21^{b}

Chromium stress and BC application significantly influenced germination traits of *Brassica juncea* ($p \leq 0.05$; Figure 6). Germination percentage was significantly reduced under Cr stress, with M2 showing significantly lower values than the Control and BC treatments. In contrast, BC alone recorded the highest germination percentage and was significantly higher than M1, M2, and BC+M2, while remaining statistically at par with the Control and BC+M1. The combined application of BC with Cr improved germination compared to Cr-only treatments, as BC+M1 and BC+M2 showed higher values than M1 and M2, respectively.

A similar trend was observed for the Seedling Vigour Index. M2 showed a significant decline compared to the Control, whereas BC alone exhibited a significantly higher vigour index than all other treatments. The BC+M1 treatment was statistically at par with the Control but significantly higher than M1, M2, and BC+M2, indicating effective amelioration under moderate stress. BC+M2 also showed improvement over M2 but remained significantly lower than the Control.

In terms of Germination Mean Time, Cr stress significantly delayed germination, with M2 showing significantly higher values than all other treatments. However, BC application significantly reduced the germination time, as BC alone recorded the lowest value and was significantly lower than M1, M2, and BC+M2, while remaining statistically similar to the Control and BC+M1.

Overall, biochar application improved germination performance and vigour while reducing the delay caused by Cr stress.

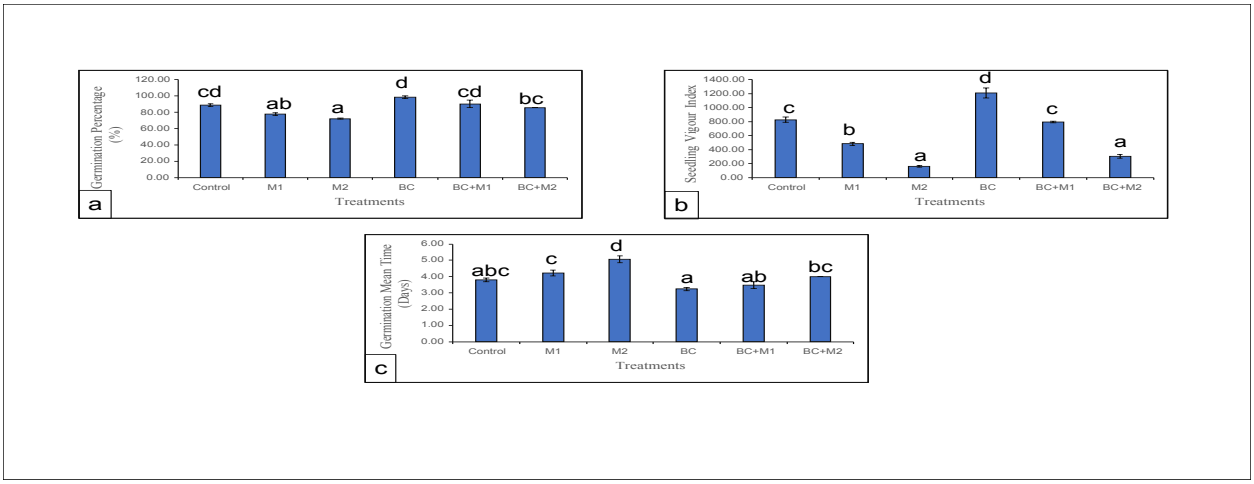

Figure 6: Effect of Biochar (BC) on (**a**) Germination Percentage (**b**) Seedling Vigour Index (**c**) Germination Mean Time in 10 days old *Brassica juncea* seedlings under chromium (M1 and M2) stress. Bars represent mean ± standard error of three replicates. Different letters above the bars indicate statistically significant differences among treatments according to Tukey's HSD test at $p < 0.05$; bars sharing the same letter are not significantly different.

3.3. Influence of Biochar on Photosynthetic Pigment Content of *Brassica juncea* Seedlings under Cr Stress

The results (Figure 7) demonstrate that Cr stress and BC application significantly affected the photosynthetic pigment content of *Brassica juncea* seedlings ($p \leq 0.05$). Chromium exposure, particularly at the higher concentration (M2), caused a significant reduction in all pigments, with chlorophyll a, chlorophyll b, total chlorophyll, and total carotenoids decreasing by 39.2%, 46.7%, 49.1%, and 50%, respectively, compared to the Control, indicating impaired photosynthetic efficiency. Both M1 and M2 recorded significantly lower pigment contents than the Control. In contrast, BC application alone significantly enhanced pigment levels, increasing chlorophyll a by 94.8%, chlorophyll b by 47.3%, total chlorophyll by 43.4%, and total carotenoids by 98.6% over the Control, and showed significantly higher values than all other treatments. Furthermore, the combined application of BC with Cr (BC+M1 and BC+M2) significantly alleviated Cr-induced pigment loss, as these treatments exhibited significantly higher pigment contents than their respective Cr-only treatments. Notably, BC+M1 showed pigment levels comparable to the Control, whereas BC+M2, although significantly improved compared to M2, remained lower than

the Control, highlighting the protective role of BC in mitigating Cr-induced damage to the photosynthetic apparatus.

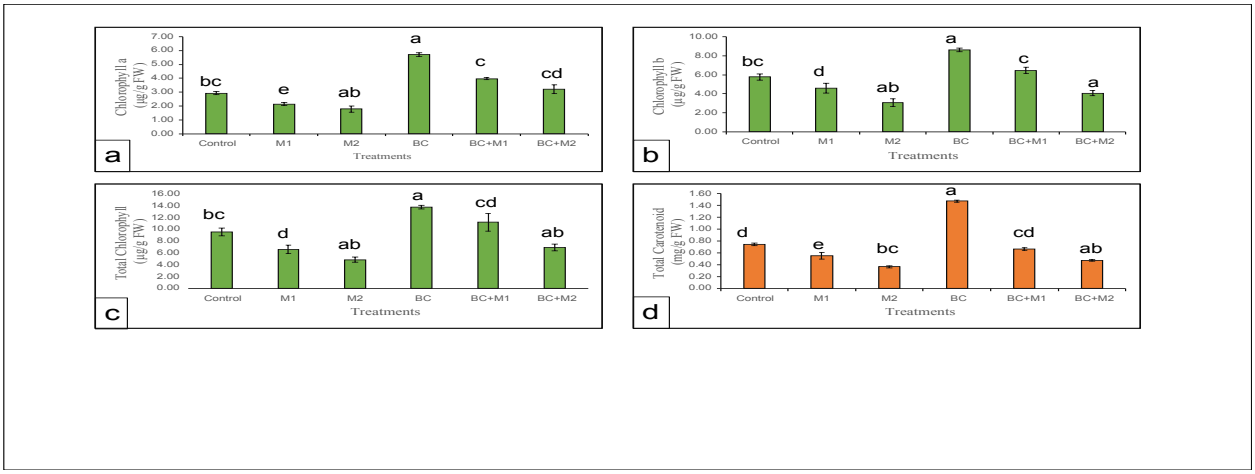

Figure 7: Effect of Biochar (BC) on (**a**) Chlorophyll a (**b**) Chlorophyll b (**c**) Total Chlorophyll (**d**) Total Carotenoid content in 10 days old *Brassica juncea* seedlings under chromium (M1 and M2) stress. Bars represent mean ± standard error of three replicates. Different letters above the bars indicate statistically significant differences among treatments according to Tukey's HSD test at $p < 0.05$; bars sharing the same letter are not significantly different.

The effect of Cr and BC treatments on pheophytin a, pheophytin b, and total pheophytin content in *Brassica juncea* seedlings is presented in Figure 8. Chromium stress significantly increased pheophytin accumulation ($p \leq 0.05$), with M2 recording the highest values, showing increases of 39.03%, 82.7%, and 45.3% in pheophytin a, pheophytin b, and total pheophytin, respectively, compared to the Control. M2 was significantly higher than all BC-amended treatments, while M1 was also significantly higher than BC, BC+M1, and BC+M2 but remained statistically similar to the Control for some parameters. In contrast, BC application alone showed the lowest pheophytin content and was significantly lower than the Control, M1, and M2. Furthermore, the combined application of BC with Cr (BC+M1 and BC+M2) significantly reduced pheophytin levels compared to their respective Cr-only treatments. BC+M1 showed values comparable to BC, whereas BC+M2 exhibited intermediate levels, being significantly lower than M2 but higher than BC. These findings indicate that Cr stress enhanced chlorophyll degradation, while BC application significantly minimized pheophytin accumulation, demonstrating its protective role against Cr-induced damage.

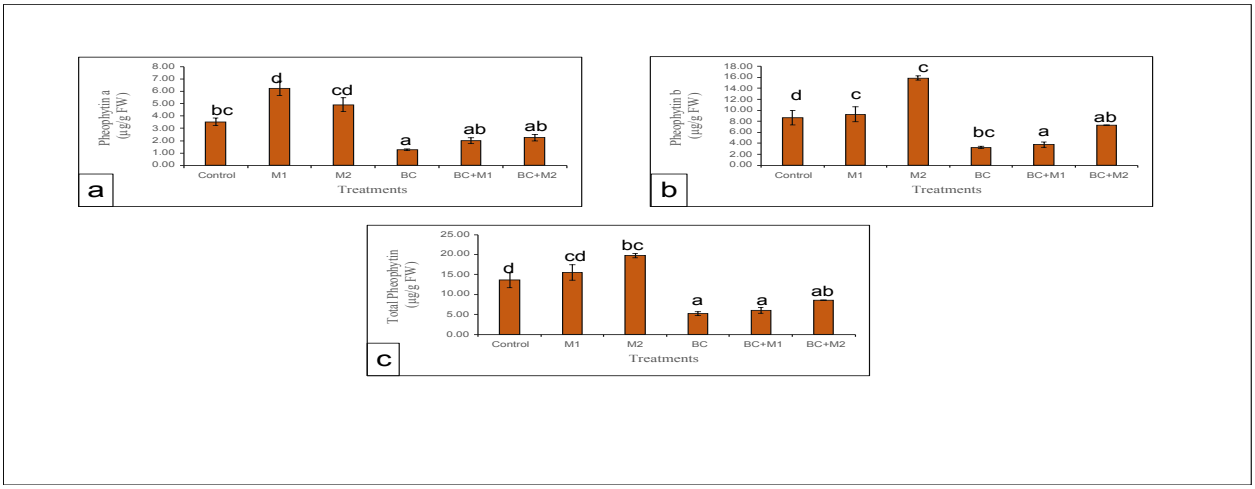

Figure 8: Effect of Biochar (BC) on (**a**) Pheophytin a (**b**) Pheophytin b (**c**) Total Pheophytin Content in 10 days old *Brassica juncea* seedlings under chromium (M1 and M2) stress. Bars represent mean ± standard error of three replicates. Different letters above the bars indicate statistically significant differences among treatments according to Tukey's HSD test at $p < 0.05$; bars sharing the same letter are not significantly different.

3.4. Influence of Biochar on Secondary Metabolites Content of *Brassica juncea* Seedlings under Cr Stress

Figure 9 shows that both Cr stress and BC application significantly affected the accumulation of secondary metabolites in *Brassica juncea* seedlings ($p \leq 0.05$). Chromium toxicity significantly increased total phenol ($F = 15.119$; $df_{between} = 5$; $df_{within} = 12$), flavonoid ($F = 58.518$; $df_{between} = 5$; $df_{within} = 12$), and anthocyanin content ($F = 29.009$; $df_{between} = 5$; $df_{within} = 12$) compared to the Control. For total phenol content, seedlings treated with M2 exhibited significantly higher levels than the Control ($p < 0.05$). A similar increasing trend was observed under the BC+M1 treatment, where total phenol levels were significantly higher than both the Control and M1 treatments ($p < 0.05$), but remained comparable to M2 ($p > 0.05$). Likewise, BC-treated seedlings showed significantly higher total phenol content than the Control ($p < 0.05$), with no significant difference compared to M2 ($p > 0.05$).

In terms of flavonoid content, a significant increase was observed in seedlings treated with M1 compared to the Control ($p < 0.05$), followed by a further significant rise under M2 treatment ($p < 0.05$). BC application also resulted in significantly higher flavonoid levels than the Control ($p < 0.05$), although values were comparable to M2 ($p > 0.05$). The combined BC+M1 treatment led to a significant enhancement over BC alone ($p < 0.05$), while the highest flavonoid content was recorded in BC+M2-treated seedlings, which was significantly greater than all other treatments ($p < 0.05$).

For anthocyanin content, BC-treated seedlings exhibited the highest levels, being significantly greater than the Control as well as all other treatments (M1, M2, BC+M1, and BC+M2) ($p < 0.05$). Seedlings under M2 showed a significant increase over the Control ($p < 0.05$), but remained statistically similar to M1 ($p > 0.05$). The BC+M1 treatment did not result in any significant change compared to the Control ($p > 0.05$), whereas BC+M2 treatment significantly increased anthocyanin levels relative to M1 ($p < 0.05$), though values were still lower than those observed with BC alone ($p < 0.05$).

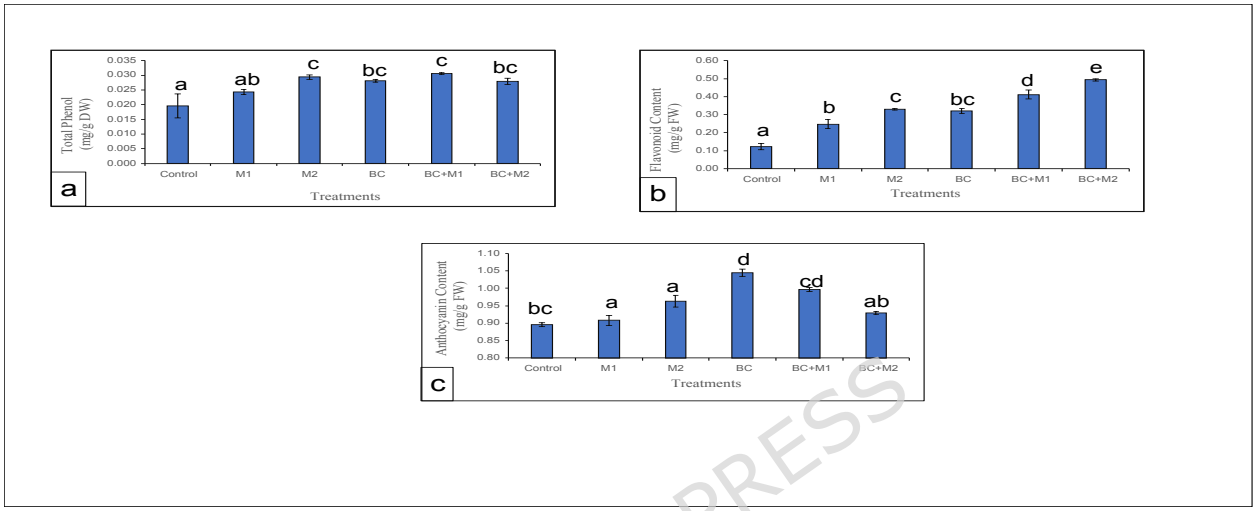

Figure 9: Effect of Biochar (BC) on (**a**) Total Phenol (**b**) Flavonoid and (**c**) Anthocyanin content in 10 days old *Brassica juncea* seedlings under chromium (M1 and M2) stress. Bars represent mean ± standard error of three replicates. Different letters above the bars indicate statistically significant differences among treatments according to Tukey's HSD test at $p < 0.05$; bars sharing the same letter are not significantly different.

3.5. Influence of Biochar on Osmolytes Content of *Brassica juncea* Seedlings under Cr Stress

The result shown in Figure 10 presents the effect of different treatments on the content of osmolytes such as total carbohydrates, trehalose and proline in *Brassica juncea* seedlings. Total carbohydrate content was significantly highest under BC alone ($p < 0.05$), followed by BC+M1, while the Control recorded the lowest value. BC+M1 was significantly higher than M2 and M1 ($p < 0.05$), whereas BC+M2 did not differ significantly from M2 ($p > 0.05$). For trehalose, M2 and BC exhibited the highest contents and were not significantly different from each other ($p > 0.05$). Both were significantly higher than M1, BC+M1, BC+M2, and the Control ($p < 0.05$). BC+M1 and BC+M2 showed intermediate values and were significantly higher than the Control ($p < 0.05$), but lower than BC and M2 ($p < 0.05$). In the case of proline, BC and BC+M2 recorded the maximum accumulation and were statistically at par ($p > 0.05$). Both were significantly higher than the Control, M1, M2, and BC+M1 ($p < 0.05$). The Control consistently showed the lowest osmolyte levels across all parameters.

4. Correlation Analysis

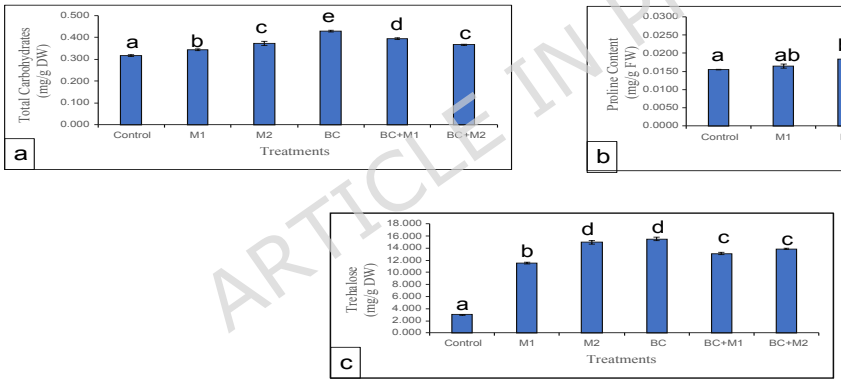

Figure 10: Effect of Biochar (BC) on (**a**) Total Carbohydrates (**b**) Proline content and (**c**) Trehalose in 10 days old *Brassica juncea* seedlings under chromium (M1 and M2) stress. Bars represent mean ± standard error of three replicates. Different letters above the bars indicate statistically significant differences among treatments according to Tukey's HSD test at $p < 0.05$; bars sharing the same letter are not significantly different.

The correlation analysis (Figure 11) revealed strong and significant relationships among growth and biochemical parameters. Growth attributes such as root length, shoot length, fresh weight, dry weight, and moisture content exhibited strong positive correlations ($r \approx 0.62–0.99$), indicating coordinated plant development and suggesting that improvement in one parameter is closely

associated with overall biomass accumulation. Similarly germination percentage, seed vigor index, and stress tolerance indices, were highly positively correlated, confirming their reliability as indicators of early plant establishment under stress conditions.

In contrast, mean germination time showed strong negative correlations with most growth and germination traits ($r \approx -0.72$ to -0.96), indicating that delayed germination adversely affects plant performance. Photosynthetic pigments, including chlorophyll a, chlorophyll b, total chlorophyll, and carotenoids, were strongly positively correlated with each other, reflecting the coordinated functioning of the photosynthetic system.

Stress-related pigments, particularly pheophytin (pheophytin a, pheophytin b, and total pheophytin), exhibited strong negative correlations with growth and chlorophyll content, indicating that increased chlorophyll degradation is associated with reduced plant health under stress conditions. The resulting accumulation of pheophytins under HM stress often coincides with heightened oxidative stress in plants thus can serve as an early indicator of Cr toxicity. Additionally, biochemical parameters such as phenols, flavonoids, anthocyanins, total carbohydrates, trehalose, and proline showed positive correlations among themselves, suggesting their coordinated accumulation under stress. However, their moderate negative association with growth traits indicates a shift in plant metabolism toward stress response rather than growth.

501

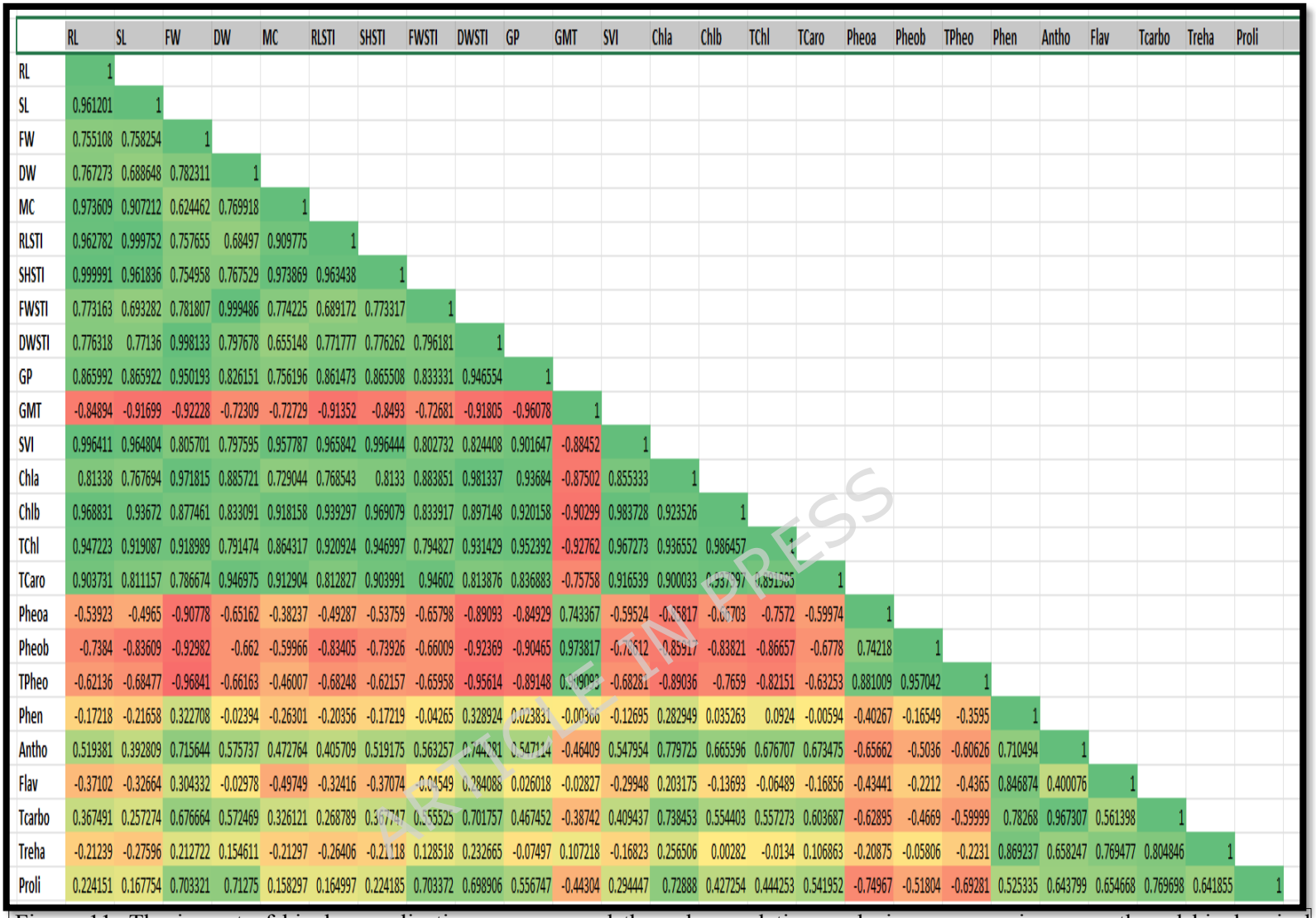

	RL	SL	FW	DW	MC	RLSTI	SHSTI	FWSTI	DWSTI	GP	GMT	SVI	Chla	Chlb	TChl	TCaro	Pheoa	Pheob	TPheo	Phen	Antho	Flav	Tcarbo	Treha	Proli
RL	1																								
SL	0.961201	1																							
FW	0.755108	0.758254	1																						
DW	0.767273	0.688648	0.782311	1																					
MC	0.973609	0.907212	0.624462	0.769918	1																				
RLSTI	0.962782	0.999752	0.757655	0.68497	0.909775	1																			
SHSTI	0.999991	0.961836	0.754958	0.767529	0.973869	0.963438	1																		
FWSTI	0.773163	0.693282	0.781807	0.999486	0.774225	0.689172	0.773317	1																	
DWSTI	0.776318	0.77136	0.998133	0.797678	0.655148	0.771777	0.776262	0.796181	1																
GP	0.865992	0.865922	0.950193	0.826151	0.756196	0.861473	0.865508	0.833331	0.946554	1															
GMT	-0.84894	-0.91699	-0.92228	-0.72309	-0.72729	-0.91352	-0.8493	-0.72681	-0.91805	-0.96078	1														
SVI	0.996411	0.964804	0.805701	0.797595	0.957787	0.965842	0.996444	0.802732	0.824408	0.901647	-0.88452	1													
Chla	0.81338	0.767694	0.971815	0.885721	0.729044	0.768543	0.8133	0.883851	0.981337	0.93684	-0.87502	0.855333	1												
Chlb	0.968831	0.93672	0.877461	0.833091	0.918158	0.939297	0.969079	0.833917	0.897148	0.920158	-0.90299	0.983728	0.923526	1											
TChl	0.947223	0.919087	0.918989	0.791474	0.864317	0.920924	0.946997	0.794827	0.931429	0.952392	-0.92762	0.967273	0.936552	0.986457	1										
TCaro	0.903731	0.811157	0.786674	0.946975	0.912904	0.812827	0.903991	0.94602	0.813876	0.836883	-0.75758	0.916539	0.900033	[illegible]	[illegible]	1									
Pheoa	-0.53923	-0.4965	-0.90778	-0.65162	-0.38237	-0.49287	-0.53759	-0.65798	-0.89093	-0.84929	0.743367	-0.59524	[illegible]	[illegible]	-0.7572	-0.59974	1								
Pheob	-0.7384	-0.83609	-0.92982	-0.662	-0.59966	-0.83405	-0.73926	-0.66009	-0.92369	-0.90465	0.973817	[illegible]	[illegible]	-0.83821	-0.86657	-0.6778	0.74218	1							
TPheo	-0.62136	-0.68477	-0.96841	-0.66163	-0.46007	-0.68248	-0.62157	-0.65958	-0.95614	-0.89148	[illegible]	-0.68281	-0.89036	-0.7659	-0.82151	-0.63253	0.881009	0.957042	1						
Phen	-0.17218	-0.21658	0.322708	-0.02394	-0.26301	-0.20356	-0.17219	-0.04265	0.328924	[illegible]	[illegible]	-0.12695	0.282949	0.035263	0.0924	-0.00594	-0.40267	-0.16549	-0.3595	1					
Antho	0.519381	0.392809	0.715644	0.575737	0.472764	0.405709	0.519175	0.563257	[illegible]	[illegible]	-0.46409	0.547954	0.779725	0.665596	0.676707	0.673475	-0.65662	-0.5036	-0.60626	0.710494	1				
Flav	-0.37102	-0.32664	0.304332	-0.02978	-0.49749	-0.32416	-0.37074	[illegible]	0.284088	0.026018	-0.02827	-0.29948	0.203175	-0.13693	-0.06489	-0.16856	-0.43441	-0.2212	-0.4365	0.846874	0.400076	1			
Tcarbo	0.367491	0.257274	0.676664	0.572469	0.326121	0.268789	[illegible]	[illegible]	0.701757	0.467452	-0.38742	0.409437	0.738453	0.554403	0.557273	0.603687	-0.62895	-0.4669	-0.59999	0.78268	0.967307	0.561398	1		
Treha	-0.21239	-0.27596	0.212722	0.154611	-0.21297	-0.26406	-0.21118	0.128518	0.232665	-0.07497	0.107218	-0.16823	0.256506	0.00282	-0.0134	0.106863	-0.20875	-0.05806	-0.2231	0.869237	0.658247	0.769477	0.804846	1	
Proli	0.224151	0.167754	0.703321	0.71275	0.158297	0.164997	0.224185	0.703372	0.698906	0.556747	-0.44304	0.294447	0.72888	0.427254	0.444253	0.541952	-0.74967	-0.51804	-0.69281	0.525335	0.643799	0.654668	0.769698	0.641855	1

Figure 11: The impact of biochar application was assessed through correlation analysis among various growth and biochemical attributes in 10 days old Cr-stressed *Brassica juncea* L. seedlings. In the correlation matrix, green shades indicate strong positive correlations, yellow indicates weak or no correlation, and red shades represent strong negative correlations between the measured parameters.

502 **Abbreviations**[1]

503 **5. Discussion**

[1] FW, Fresh Weight; DW, Dry Weight; RL, Root length; SL, Shoot Length; MC, Moisture Content; DWSTI, Dry Weight Stress Tolerance Index; Fresh Weight Stress Tolerance Index; RLSTI, Root Length Stress Tolerance Index; SHSTI, Shoot Height Stress Tolerance Index; FWSTI, GP, Germination Percentage; GMT, Germination Mean Time; SVI, Seedling Vigor Index; Chla, Chlorophyll a; Chlb, Chlorophyll; Tchl, Total Chlorophyll; TCaro, Total Carotenoids; Pheoa, Pheophytin a; Pheob, Pheophytin b; Tpheo, Total Pheophytin; Phen, Total Phenol; Antho, Anthocyanin; Flav, Flavonoid; TCarbo, Total Carbohydrate; Treha, Trehalose; Proli, Proline

The aim of study was to investigate the metal-sequestering potential of apricot kernel shell-derived BC and to elucidate the mechanisms by which it mitigates Cr-induced phytotoxicity, with a particular focus on plant growth parameters, photosynthetic pigment content, secondary metabolites and osmolytes.

5.1. Biochar Properties and Cr Immobilization Mechanisms

In the present study, the apricot kernel shell–derived BC exhibited a pH of 7.84, reflecting its alkaline nature, which is a characteristic feature of BC produced from such lignocellulosic biomass. The shift toward a near-neutral to alkaline pH is characteristic of pyrolysis in the 500–550°C range; this occurs as alkali salts begin to separate from the organic matrix above 300°C, leading to a concentrated accumulation of alkali earth metals within the resulting carbon structure (Tomczyk et al., 2020; Yu et al., 2014). This alkalinity is instrumental in neutralizing acidic soils and markedly affects the mobility and availability of HMs. As soil pH rises, HMs bind more strongly to soil particles, leading to reduced mobility and lower uptake by plants. (Su et al., 2024; Amin et al., 2023; Meng et al., 2023; Yuan et al., 2021). Moreover, elevated soil pH can promote the formation of metal hydroxide precipitates, further decrease their bioavailability and contribute to HM immobilization (Singh et al., 2010). FTIR spectra (Figure 2) confirmed the presence of several surface functional groups, including C–C, C–H, C–O, and –C=O, indicating the enriched organic carbon structure of BC and highlighting its potential as an effective soil rejuvenator (Zhang et al., 2021; Zhang et al., 2018). These surface functionalities enhance the adsorption of heavy metals by facilitating hydrogen bonding and other surface interactions with metal ions (Huang et al., 2021; Wu et al., 2020). Abbas et al. (2018) reported that groups such as C–C, C–O, and –COOH contribute significantly to HM immobilization through ion-exchange processes. Moreover, heteroatoms such as oxygen and hydrogen present in –OH and –COOH groups can act as coordination sites that promote complex formation with HM ions, thereby stabilizing them on the BC surface (Li et al., 2020; Zhu et al., 2019). In addition to adsorption mechanisms, redox reactions also play an important role in Cr immobilization. Electron-shuttle experiments conducted by Xu et al. (2019) demonstrated that –C–O and –C=O groups present on the BC surface function as electron-donating sites that facilitate the reduction of Cr(VI) to the less toxic Cr(III) form. These groups, commonly present as phenolic, ketonic, and amino structures, can donate electrons during oxidation reactions, leading to their transformation into quinone groups and ammonium salts. This

electron-transfer process promotes the conversion of Cr(VI) to Cr(III), thereby decreasing its toxicity, mobility, and bioavailability The zeta potential of the BC was recorded as –22.3 mV, indicating a negatively charged surface. This negative zeta potential is attributed to the presence of oxygen-containing functional groups, such as carboxylate (–COO□) and hydroxyl (–OH), on the BC surface, which impart electronegativity (Nicholas et al., 2022). These oxygen-containing functional groups can donate electrons and facilitate the reduction of Cr(VI) to Cr(III) (Guo et al., 2020). During this redox process, C–O and C=O groups were oxidized into carboxylic (–COOH) groups, indicating electron transfer from BC to Cr (Xu et al., 2019). The generated Cr^{3}□ is subsequently immobilized through ion exchange or surface complexation mechanisms, as proposed by Lyubchik et al. (2004), where Cr^{3}□ may exchange with inherent cations such as K□ present on the BC surface, resulting in its stabilization and immobilization. The FESEM analysis showed that the BC possessed a highly porous surface, which helps in the physical adsorption of heavy metals (Emamverdian et al., 2025; Liang et al., 2021). Furthermore, the porous architecture of BC provides abundant active sites that serve as a microhabitat for microbial colonization, enhancing microbial survival and activity under stress conditions. This microbial–biochar system improves soil properties by increasing organic carbon content and cation exchange capacity, while reducing redox potential and bulk density. Consequently, microbial activity, together with interactions with the BC matrix, significantly contributes to heavy metal immobilization, resulting in reduction of Cr(VI) to Cr(III) and a substantial increase in the stable residual fraction of Cr (Bolan et al., 2023; Chen et al., 2021). The XRD spectra of apricot shell-derived BC synthesized at 500°C exhibited a predominantly amorphous nature. At this moderate carbonization temperature, the BC matrix preserves a high density of oxygen-containing functional groups, which serve as essential active sites for HM interaction. However, as the pyrolysis temperature increases, the BC undergoes a structural transition toward graphitic crystallinity, evidenced by the narrowing of XRD peaks. This structural ordering is accompanied by a significant reduction in oxygen-containing functional groups abundance due to thermal deoxygenation and decarboxylation, ultimately diminishing the BC's capacity for the adsorption-coupled reduction of Cr(VI) (Somboon et al., 2025; Nguyen et al., 2024; Edeh et al., 2023). The apricot shell derived BC exhibited a BET surface area of 1.387 m^2/g. Although high BET surface area is often considered advantageous for HM adsorption, but several studies for instance, Dong et al. (2025); Daffalla, (2023); Hossain et al. (2020); demonstrate that BC with relatively low surface area can

still effectively mitigate Cr phytotoxicity. This is because metal immobilization is governed not only by physical adsorption but also by surface functional groups, mineral constituents, alkalinity, and redox reactions that convert toxic Cr(VI) into less mobile Cr(III).

5.2. Impact on Plant Growth and Germination

Cr contamination in soil has been shown to negatively impact plant physiological processes, particularly germination and growth in *Brassica juncea* plants (Kour et al., 2024). In the current study. Cr exposure significantly reduced germination percentage, seedling vigour, and prolonged the time required for seed germination, consistent with previous reports (Iqbal et al., 2023; Siddiqui et al., 2014). Similarly, notable reductions in both root and shoot lengths were observed under Cr stress, in agreement with findings in other plant species such as *Triticum aestivum* and *Solanum lycopersicum*, which also exhibited growth inhibition (Devi et al., 2024; Kumar et al., 2022).The decline in root development may be attributed to disrupted cell division and alterations in cell cycle regulatory genes, often resulting in chromosomal abnormalities (Kundu et al., 2018; Yang et al., 2017). Such impaired root systems limit water and nutrient uptake, subsequently affecting shoot elongation (Mukta et al., 2019; Rajendran et al., 2019; Shahid et al., 2017). Furthermore, the study observed a significant decrease of fresh and dry matter in *Brassica juncea* seedlings exposed to Cr, reflecting the physiological stress imposed by Cr toxicity (Bashir et al., 2021; González et al., 2015). However, the application of BC has increased germination percentage (Karim et al., 2025;) and reduced germination mean time (Ali et al., 2021; Qayyum et al., 2015) by improving soil physicochemical properties. Its porous structure enhances soil water-holding capacity and moisture availability, which promotes rapid seed imbibition and accelerates germination (Al Hinai et al., 2023; Pehlivan and Wang, 2022; Basso et al. 2013; Kammann et al. 2011). In addition, BC supplies slow-release mineral nutrients and improves soil fertility, thereby supporting early metabolic activities required for germination (Yang et al., 2015). These improvements create a favorable environment for seedling emergence and plant growth while simultaneously reducing the bioavailability of toxic metals in soil (Emamverdian et al., 2024; Calcan et al., 2022).

5.3. Modulation of Photosynthetic Apparatus

For the early detection of HM toxicity in plants, organic compounds such as chlorophylls serve as reliable bio-indicators. Since chlorophyll plays a key role in photosynthesis, assessing its content provides valuable insights into the physiological effects of metal stress. In the present study,

increasing concentrations of Cr significantly declined the content of chlorophyll *a* and *b,* total chlorophyll and total carotenoid. This trend reflects the disruptive effect of HMs on key metabolic processes, particularly through the inactivation of enzymes essential for normal cellular functions. Given that chlorophylls are integral to the pigment system within chloroplasts, their reduction directly impairs plant growth (Pourakbar et al., 2007). The observed decline in chlorophyll content may be attributed to the inhibition of key enzymes involved in the synthesis of chlorophyll, such as protochlorophyllide reductase and aminolevulinic acid dehydratase (Adamczyk-Szabela et al., 2023). Similar reductions in photosynthetic pigment levels under Cr stress have also been documented in *Helianthus annuus* L. (Ramzan et al., 2023), *Vicia faba* L. (Bouhadi et al., 2024) and *Raphanus sativus* (Younis et al., 2024), supporting the findings of the current study. However, the application of BC, both individually and in combination with Cr, alleviated the stress caused by the metal, as evidenced by the enhanced levels of all photosynthetic pigments analyzed in the present study. Our findings align with those of Younis et al. (2024), who observed that applying 0.75% BC increased chlorophyll a by 12.66%, chlorophyll b by 40.67%, total chlorophyll by 20.84%, and carotenoid content by 48.19% in *Cr*-stressed *Raphanus sativus*. Similarly, 5% cotton stalk and 3% sugarcane bagasse-derived BC enhanced the photosynthetic pigment content in *Spinacia oleracea L.* and *Zea mays L.* respectively under Cr stress (Sami et al., 2023; Bashir et al., 2021).

5.4. Induction of Secondary Metabolism and Osmoprotection

Phenolic compounds exhibit strong redox activity and function as effective antioxidants under stress conditions by scavenging ROS and stabilizing cellular redox homeostasis (Vallverdú-Queralt et al., 2014). Their biosynthesis is primarily regulated through the phenylpropanoid pathway, where phenylalanine acts as a central precursor for a wide range of secondary metabolites, including flavonoids, anthocyanins, lignins, phytoalexins, and phenolic acids. Under HM stress, the activation of this pathway represents a crucial adaptive response, as plants enhance the synthesis of these compounds to counteract oxidative damage and metal toxicity (Sharma et al., 2025; Anjitha et al., 2021). This upregulation is largely mediated by increased activity of key enzymes such as phenylalanine ammonia-lyase (PAL), shikimate dehydrogenase, and polyphenol oxidase, which collectively drive the accumulation of phenolic metabolites (Zoufan et al., 2020; Kaur et al., 2017). These metabolites not only function as antioxidants but also participate in metal

chelation, cell wall strengthening (*via* lignification), and restriction of metal translocation, thereby contributing to Cr immobilization within plant tissues.

In addition to phenolics, the accumulation of soluble sugars and osmolytes represents another critical defense strategy under stress conditions. Sugars such as sucrose, trehalose, hexoses, and raffinose family oligosaccharides act as osmoprotectants, signaling molecules, and metabolic regulators, helping to maintain cellular integrity and osmotic balance. These compounds play a vital role in stabilizing membranes and proteins, preserving photosynthetic machinery, and mitigating oxidative damage by directly or indirectly scavenging ROS (Ahmad et al., 2020). Furthermore, soluble carbohydrates serve as essential sources of energy and carbon skeletons required for sustaining metabolic processes and synthesizing stress-responsive biomolecules. Their accumulation is closely associated with improved membrane stability and maintenance of turgor pressure, which are essential for plant survival under Cr-induced stress (Emamverdian et al., 2025; Arno and Hernández-Ruiz, 2019).

The findings of the present study are consistent with previous reports demonstrating enhanced accumulation of secondary metabolites and osmolytes under HM stress and BC application, such as in bamboo (Emamverdian et al., 2025), tomato (Anbuganesan et al., 2024; Badawy et al., 2022), medicinal herbs (Nigam et al., 2021), cowpea (Phares et al., 2020), peanut (Chen et al., 2020), and lettuce (Quartacci et al., 2017). Collectively, these results suggest that the accumulation of phenolic compounds and soluble sugars is not merely a stress symptom but a coordinated adaptive mechanism that enhances plant tolerance by integrating antioxidant defense, osmotic regulation, and metabolic stability under HM stress conditions.

6. Future Research Directions

Research on the ability of BC to reduce HM toxicity in plants is an area of increasing research interest. The results of the present study demonstrate the effectiveness of BC in alleviating Cr phytotoxicity through improvements in growth and biochemical parameters. In the present study, Cr stress reduced chlorophyll content, whereas the application of BC, either alone or in combination with Cr, enhanced pigment levels compared with the stress treatment. Future studies should investigate the effects of these treatments on δ-aminolevulinic acid and glutamate-1-semialdehyde, which are key intermediates in the tetrapyrrole biosynthesis pathway. Similarly, the activity of phenylalanine ammonia-lyase, a key regulatory enzyme of the phenylpropanoid

pathway responsible for the synthesis of various secondary metabolites involved in plant defense, stress tolerance, and structural support, should also be examined.

Future endeavors should also analyze the expression patterns of key HM responsive genes involved in photosynthesis, energy metabolism, and secondary metabolite biosynthesis. Detailed transcriptional studies targeting photosynthetic genes such as *PetH* (photosystem I) and *LHCB7* (photosystem II), as well as the chloroplast ATP synthase gene *atpD*, would provide deeper insight into the physiological adjustments induced by BC under heavy metal exposure. Furthermore, gene expression analysis of metabolic pathways associated with plant defence and detoxification particularly phenylpropanoid metabolism (*HCT*, *COMT*) and flavonoid biosynthesis (*FG3*, *GT1*, *CHS*, *FLS*) should be undertaken.

To better understand the mechanisms governing BC–Cr interactions, detailed kinetic investigations are required to elucidate the rate, pathways, and controlling mechanisms of Cr immobilization by BC. Furthermore, the assessment of soil enzyme activities, particularly dehydrogenase, urease, and phosphatases, should be prioritized to clarify the relationship between microbial functional recovery, soil fertility, and plant performance. Additionally, integrating the above measured biochemical indicators with multi-omics approaches, including metagenomics, metatranscriptomics, and metabolomics, would provide a holistic framework to decode biochar–microbe–plant interactions and support the development of effective and sustainable remediation strategies for Cr-contaminated soils.

7. Conclusion

HM toxicity is a growing concern that adversely affects the growth and development of plants. In the present study, apricot kernel shell BC, procured from the Kargil district of UT Ladakh, was used to ameliorate Cr toxicity in *Brassica juncea* seedlings. Characterization of this BC revealed that its alkaline nature, negative zeta potential, and abundance of functional groups impart it with the potential to reduce Cr phytotoxicity. This was further confirmed by the positive responses observed in various growth and biochemical parameters under treatments with Cr, BC, and their combination (Figure 12), where compared to control, the application of 1% BC had increased root length by 24.75%, shoot length (35.91%), fresh weight (57.12%) and dry weight (133.3%). Similar kind of positive effect was also observed in the photosynthetic pigments (Chlorophyll a, Chlorophyll b, Total Chlorophyll and Total Carotenoids). Furthermore, content of secondary

metabolites and osmolytes were also estimated, their results again demonstrated the effectiveness of BC in alleviating Cr phytotoxicity. Overall, BC application improved all measured parameters, indicating that apricot kernel shell-derived BC can serve as a promising eco-friendly amendment for the amelioration of Cr stress in plants.

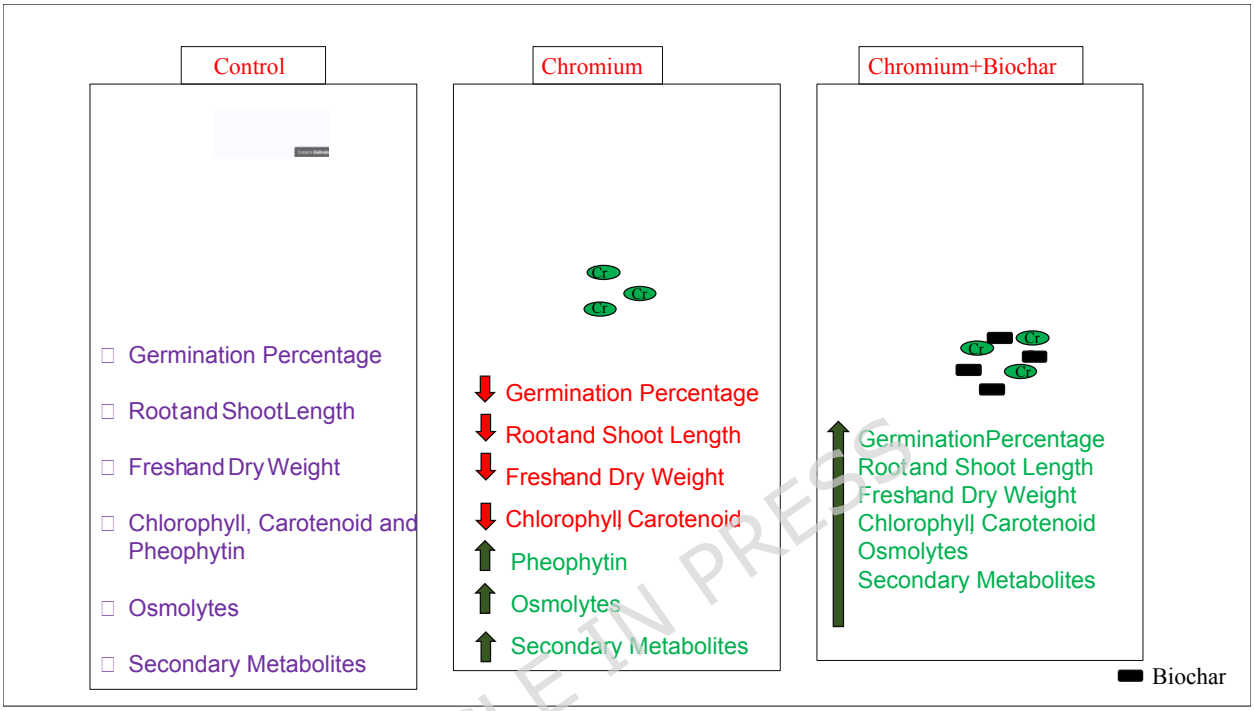

Figure 12: Schematic illustration depicting the effects of Cr stress and biochar application on growth, germination, and biochemical attributes of *Brassica juncea* L. seedlings.

Acknowledgement

The author duly acknowledged the University Grant Commission, Government of India, for its financial support through the Senior Research Fellowship (SRF). The authors also express their gratitude to DBT, DST-PURSE, DST-FIST and Centre of Emerging Life Sciences, GNDU, Amritsar, India for providing the required facilities and support.

Data Availability

The original findings given in the study are provided in the article material. Further inquiries, if any should be made to the corresponding author.

Contributions

N.R.M.: Conceptualization, drafting, methodology, acquisition of data, data curation, formal analysis, writing—review and editing. M.S.M.: Provided facility for the preparation of biochar N.K.: Conceptualization, Supervision, visualization, editing and validation.

Funding Declaration

No Funding

Reference

Abdelhameed, R. E., and Metwally, R. A. The potential utilization of mycorrhizal fungi and glycine betaine to boost the fenugreek (*Trigonella foenum-graecum* L.) tolerance to chromium toxicity. *Journal of Soil Science and Plant Nutrition*, **25**(1), 259-278 (2025).

Adamczyk-Szabela, D. et al. Antioxidant activity and photosynthesis efficiency in Melissa officinalis subjected to heavy metals stress. *Molecules*, **28**(6), 2642 (2023).

Ahmad, F., Singh, A., and Kamal, A. Osmoprotective role of sugar in mitigating abiotic stress in plants. In: Roychoudhury, A., Durgesh Kumar Tripathi, D.K. (Eds). Protective chemical agents in the amelioration of plant abiotic stress: biochemical and molecular perspectives, 53-70 (2020).

Ai, T., Jiang, X., and Liu, Q. Chromium removal from industrial wastewater using Phyllostachys pubescens biomass loaded Cu-S nanospheres. *Open Chemistry*, **16**(1), 842-852 (2018).

Akram, N. A. et al. Foliage application and seed priming with nitric oxide causes mitigation of salinity-induced metabolic adversaries in broccoli (*Brassica oleracea* L.) plants. *Acta Physiologiae Plantarum*, **42**(10), 155. (2020).

Al Hinai, M. et al. Co-application of biochar and seed priming with nano-sized chitosan-proline improves salt tolerance in differentially responding bread wheat genotypes. *Journal of Soil Science and Plant Nutrition*, **23**(3), 3058-3073 (2023).

Al-Huqail, A. A. et al. Ascorbic acid is essential for inducing chromium (VI) toxicity tolerance in tomato roots. *Journal of Biotechnology*, **322**, 66-73. (2020a).

Al-Huqail, A. A. et al. Exogenous melatonin mitigates boron toxicity in wheat. *Ecotoxicology and Environmental Safety*, **201**, 110822. (2020b).

Ali, L. et al. Impact of biochar application on germination behavior and early growth of maize seedlings: insights from a growth room experiment. *Applied Sciences*, **11**(24), 11666 (2021).

Ali, S. et al. Effects of biochar on growth, photosynthesis, and chromium (Cr) uptake in Brassica rapa L. under Cr stress. *Arabian Journal of Geosciences*, **11**(17), 507. (2018).

Al-Wabel, M. I. et al. Conocarpus biochar as a soil amendment for reducing heavy metal availability and uptake by maize plants. *Saudi journal of biological sciences*, **22**(4), 503-511. (2015).

Ambaye, T. G. et al. Mechanisms and adsorption capacities of biochar for the removal of organic and inorganic pollutants from industrial wastewater. *International Journal of Environmental Science and Technology*, **18**(10), 3273-3294 (2021).

Amin, M. A. et al. Different feedstocks of biochar affected the bioavailability and uptake of heavy metals by wheat (Triticum aestivum L.) plants grown in metal contaminated soil. *Environmental Research*, **217**, 114845 (2023).

Anbuganesan, V. et al. Combined application of biochar and plant growth-promoting rhizobacteria improves heavy metal and drought stress tolerance in Zea mays. *Plants*, **13**(8), 1143 (2024).

Anjitha, K. S., Sameena, P. P., and Puthur, J. T. Functional aspects of plant secondary metabolites in metal stress tolerance and their importance in pharmacology. *Plant Stress*, **2**, 100038 (2021).

Arnao, M. B., and Hernández-Ruiz, J. Melatonin: a new plant hormone and/or a plant master regulator? *Trends in Plant Science*, **24**(1), 38-48 (2019).

Askari, S. H. et al. Menadione sodium bisulfite alleviated chromium effects on wheat by regulating oxidative defense, chromium speciation, and ion homeostasis. *Environmental Science and Pollution Research*, **28**(27), 36205-36225 (2021).

753 Azeem, M. et al. Removal of potentially toxic elements from contaminated soil and water using
754 bone char compared to plant-and bone-derived biochars: A review. *Journal of Hazardous*
755 *Materials*, **427**, 128131 (2022).

756 Badawy, I. H. et al. Alleviation of cadmium and nickel toxicity and phyto-stimulation of tomato
757 plant l. by endophytic Micrococcus luteus and Enterobacter cloacae. *Plants*, **11**(15), 2018 (2022).

758 Bashir, M. A. et al. Biochar mediated-alleviation of chromium stress and growth improvement of
759 different maize cultivars in tannery polluted soils. *International Journal of Environmental*
760 *Research and Public Health*, **18**(9), 4461 (2021).

761 Bashir, M. A. et al. Combined application of biochar and sulfur regulated growth, physiological,
762 antioxidant responses and Cr removal capacity of maize (*Zea mays* L.) in tannery polluted
763 soils. *Journal of environmental management*, **259**, 110051 (2020).

764 Basso, A. S. et al. Assessing potential of biochar for increasing water□holding capacity of sandy
765 soils. *Global Change Biology Bioenergy*, **5**(2), 132-143 (2013).

766 Bates, L. S., Waldren, R. P. A., and Teare, I. D. Rapid determination of free proline for water-
767 stress studies. *Plant and soil*, **39**(1), 205-207 (1973).

768 Bina, F., and Bostani, A. Effect of Salinity (NaCl) stress on germination and early seedling growth
769 of three medicinal plant species. *Advancements in Life Sciences*, **4**(3), 77-83 (2017).

770 Bolan, S. et al. The potential of biochar as a microbial carrier for agricultural and environmental
771 applications. *Science of the Total Environment*, **886,** 163968 (2023).

772 Bouhadi, M. et al. Study of the Toxicity and Translocation of Chromium (VI) in Vicia faba
773 Plant. *Bulletin of environmental contamination and toxicology*, **112**(3), 40 (2024).

774 Calcan et al. "Effects of biochar on soil properties and tomato growth." *Agronomy* **12**,(8), 1824
775 (2022).

776 Castan, S. et al. Biochar particle aggregation in soil pore water: The influence of ionic strength
777 and interactions with pyrene. *Environmental Science: Processes & Impacts*, **21**(10), 1722-1728
778 (2019).

779 Chen, X. et al. Effects of biochar and crop straws on the bioavailability of cadmium in
780 contaminated soil. *Scientific Reports*, **10**(1), 9528 (2020).

781 Chen, Y. et al. Remediation of chromium-contaminated soil based on Bacillus cereus WHX-1
782 immobilized on biochar: Cr (VI) transformation and functional microbial enrichment. *Frontiers in*
783 *microbiology*, **12**, 641913 (2021).

784 Choppala, G. et al. Differential effect of biochar upon reduction-induced mobility and
785 bioavailability of arsenate and chromate. *Chemosphere*, **144**, 374-381 (2016).

786 Close, D. C., and Wilson, S. J. Provenance effects on pre-germination treatments for Eucalyptus
787 regnans and E. delegatensis seed. *Forest Ecology and Management*, **170**(1-3), 299-305 (2002).

788 Daffalla, S. Adsorption of chromium (VI) from aqueous solution using palm leaf-derived biochar:
789 kinetic and isothermal studies. *Separations*, **10**(4), 260 (2023).

790 Devi, K. et al. Plant-derived biochar and salicylic acid as biostimulants for lycopersicon
791 esculentum under chromium toxicity conditions: insights from physiochemical attributes,
792 antioxidants, and relative gene expression. *Journal of Environmental Chemical*
793 *Engineering*, **12**(6), 114372 (2024).

794 Dong, M. et al. Biochar-amended nutrient film technique flow system effectively alleviated
795 chromium stress in guar (Cyamopsis tetragonoloba) plants. *Industrial Crops and Products*, **230**,
796 121151(2025).

797 Duwiejuah, A. B. et al. Review of biochar properties and remediation of metal pollution of water
798 and soil. *Journal of Health and Pollution*, **10**(27), 200902 (2020).

799 Edeh, I. G., Masek, O., and Fusseis, F. 4D structural changes and pore network model of biomass
800 during pyrolysis. *Scientific Reports*, **13**(1), 22863 (2023).

801 El Far, M. M., and Taie, H. A. Antioxidant activities, total anthocyanins, phenolics and flavonoids
802 contents of some sweetpotato genotypes under stress of different concentrations of sucrose and
803 sorbitol. *Australian Journal of Basic and Applied Sciences*, **3**(4), 3609-3616 (2009).

804 Ellis, R. H., and Roberts, E. H. The quantification of ageing and survival in orthodox seeds. Seed
805 Science and Technology (Netherlands), **9**(2), (1981).

Emamverdian, A. et al. Bamboo biochar helps minimize Brassica phytotoxicity driven by toxic metals in naturally polluted soils of four mine zones. *Environmental Technology & Innovation*, **36**, 103753 (2024).

Emamverdian, A. et al. Dual application of β-sitosterol and biochar reduces copper toxicity in bamboo via improved redox homeostasis. *Frontiers in Plant Science*, **16**, 1554519 (2025).

Emamverdian, A. et al. Enhanced Cd Tolerance in Bamboo: Synergistic Effects of Nano-Hydroxyapatite and Fe3O4 Nanoparticles on Reactive Oxygen Species Scavenging, Cd Detoxification, and Water Balance. *Agronomy*, **15**(2), 386 (2025).

Emamverdian, A. et al. Utilizing nano-biochar and biochar for sustainable heavy metal remediation and enhanced crop tolerance: Innovative approaches in nano-biosensing and environmental health. *Industrial Crops and Products*, **234**, 121462 (2025).

Ghandali, M. et al. Heavy metals immobilization and bioavailability in multi-metal contaminated soil under ryegrass cultivation as affected by ZnO and MnO2 nanoparticle-modified biochar. *Scientific Reports*, **14**(1), 10684 (2024).

Gong, H. et al. A review of pristine and modified biochar immobilizing typical heavy metals in soil: Applications and challenges. *Journal of Hazardous Materials*, **432**, 128668 (2022).

González, A., Gil-Díaz, M., and Lobo, M. C. Response of two barley cultivars to increasing concentrations of cadmium or chromium in soil during the growing period. *Biological trace element research*, **163**(1), 235-243 (2015).

Guo, X. et al. Adsorption mechanism of hexavalent chromium on biochar: kinetic, thermodynamic, and characterization studies. *American Chemical Society Omega* **5**, 27323–27331 (2020).

Gupta, P. et al. Implications of plant growth promoting Klebsiella sp. CPSB4 and Enterobacter sp. CPSB49 in luxuriant growth of tomato plants under chromium stress. *Chemosphere*, **240**, 124944 (2020).

Haider, F. U. et al. Biochar application for the remediation of trace metals in contaminated soils: Implications for stress tolerance and crop production. *Ecotoxicology and Environmental Safety*, **230**, 113165 (2022).

Hedge, J. E., Hofreiter, B. T., and Whistler, R. L. Carbohydrate chemistry. *Academic Press, New York*, **17**, 371-380 (1962).

Hossain, N. et al. Synthesis and characterization of rice husk biochar via hydrothermal carbonization for wastewater treatment and biofuel production. *Scientific reports*, **10**(1), 18851 (2020).

Hossain, N. et al. Synthesis and characterization of rice husk biochar via hydrothermal carbonization for wastewater treatment and biofuel production. *Scientific reports*, **10**(1), 18851 (2020).

Huang, H. et al. Efficient activation of persulfate by a magnetic recyclable rape straw biochar catalyst for the degradation of tetracycline hydrochloride in water. *Science of the Total Environment*, **758**, 143957 (2021).

Huang, Q. et al. Silicon dioxide nanoparticles enhance plant growth, photosynthetic performance, and antioxidants defence machinery through suppressing chromium uptake in Brassica napus L. *Environmental pollution*, **342**, 123013 (2024).

Hussain, S. et al. Comparative assessment of vegetable yield with and without biochar derived from locally sourced apricot shells. *Scientific Reports*, **15**(1), 6825 (2025).

Iqbal, M. Z., Murtaza, S., and Shafiq, M. Effects of chromium stress on seed germination and early seedling growth performances of pearl millet pennisetum glaucum (l.) R. Br.(poaceae). *Journal of Plant Development*, **30** (2023).

Irumva, O. et al. Environmental Fate, Transport, Impacts, and Future Perspectives of Engineered Nanoparticles in Surface Waters. *Environmental Research*, 122267 (2025).

Kammann, C. I. et al. Influence of biochar on drought tolerance of Chenopodium quinoa Willd and on soil–plant relations. *Plant and soil*, **345**(1), 195-210 (2011).

Karim, M. R. et al. Biochar enhances seed germination and crop early growth for sustainable agriculture in Bangladesh. *Public Library of Science ONE*, **20**(3), e0320005 (2025).

Kaur, P. et al. Effect of earthworms on growth, photosynthetic efficiency and metal uptake in Brassica juncea L. plants grown in cadmium-polluted soils. *Environmental Science and Pollution Research*, **24**(15), 13452-13465 (2017).

Kour, J. et al. Phytomelatonin maintained chromium toxicity induced oxidative burst in Brassica juncea L. through improving antioxidant system and gene expression. *Environmental Pollution*, **356**, 124256 (2024).

Ksheminska, H. et al. Chromium (III) and (VI) tolerance and bioaccumulation in yeast: a survey of cellular chromium content in selected strains of representative genera. *Process Biochemistry*, **40**(5), 1565-1572 (2005).

Kumar, S. et al. Chromium induces toxicity at different phenotypic, physiological, biochemical, and ultrastructural levels in Sweet potato (Ipomoea batatas L.) plants. *International Journal of Molecular Sciences*, **23**(21), 13496 (2022).

Kundu, D., Dey, S., and Raychaudhuri, S. S. Chromium (VI)–induced stress response in the plant Plantago ovata Forsk in vitro. *Genes and Environment*, **40**, 1-13 (2018).

Kushwaha, B. K. et al. Nitric oxide-mediated regulation of sub-cellular chromium distribution, ascorbate–glutathione cycle and glutathione biosynthesis in tomato roots under chromium (VI) toxicity. *Journal of Biotechnology*, **318**, 68-77 (2020).

Li, G. F. et al. A spectra metrology insight into the binding characteristics of Cu^{2+} onto anammox extracellular polymeric substances. *Chemical Engineering Journal*, **393**, 124800 (2020).

Liang, M. et al. Applications of biochar and modified biochar in heavy metal contaminated soil: A descriptive review. *Sustainability*, **13**(24), 14041 (2021).

Lichtenthaler, H. K. Chlorophylls and carotenoids: pigments of photosynthetic biomembranes. In *Methods in enzymology*. **148**, 350-382 Academic Press (1987).

Long, X. et al. Adsorption characteristics of heavy metals Pb^{2+} and Zn^{2+} by magnetic biochar obtained from modified AMD sludge. *Toxics*, **11**(7), 590 (2023).

Lu, H. et al. Relative distribution of Pb^{2+} sorption mechanisms by sludge-derived biochar. *Water research*, **46**(3), 854-862 (2012).

Lyubchik, S. I. et al. Kinetics and thermodynamics of the Cr (III) adsorption on the activated carbon from co-mingled wastes. *Colloids and Surfaces A: Physicochemical and Engineering Aspects*, **242(1-3)**, 151-158 (2004).

Maclachlan, S., and Zalik, S. Plastid structure, chlorophyll concentration, and free amino acid composition of a chlorophyll mutant of barley. *Canadian Journal of Botany*, **41**(7), 1053-1062 (1963).

Mancinelli, A. L. Interaction between light quality and light quantity in the photoregulation of anthocyanin production. *Plant Physiology*, **92**(4), 1191-1195 (1990).

Mandal, S. et al. Enhancement of chromate reduction in soils by surface modified biochar. *Journal of Environmental Management*, **186**, 277-284 (2017).

Masuku, M. et al. Pinecone biochar for the Adsorption of chromium (VI) from wastewater: Kinetics, thermodynamics, and adsorbent regeneration. *Environmental Research*, **258**, 119423 (2024).

Meng, Z. et al. Competitive adsorption and immobilization of Cd, Ni, and Cu by biochar in unsaturated soils under single-, binary-, and ternary-metal systems. *Journal of Hazardous Materials*, **451**, 131106 (2023).

Mokubung, K. E. et al. Pine cone derived polyethersulfone/biochar-Fe3O4 mixed matrix membranes for removal of arsenic from acid mine drainage. *Chemical Engineering Research and Design*, **201**, 31-44 (2024).

Mukta, R. H. et al. Calcium induces phytochelatin accumulation to cope with chromium toxicity in rice (Oryza sativa L.). *Journal of Plant Interactions*, **14**(1), 295-302 (2019).

Nguyen, D. K. et al. Adsorption mechanism of aqueous Cr (vi) by Vietnamese corncob biochar: a spectroscopic study. *Royal Society of Chemistry Advances*, **14**(53), 39205-39218 (2024).

Nguyen, D. K.et al. Adsorption mechanism of aqueous Cr (vi) by Vietnamese corncob biochar: a spectroscopic study. *RSC advances*, **14**(53), 39205-39218 (2024).

Nicholas, H. L. et al. Physico-chemical properties of waste derived biochar from community scale faecal sludge treatment plants. *Gates Open Research*, **6**, 96 (2022).

913 Nigam, N. et al. Biochar amendment reduced the risk associated with metal uptake and improved
914 metabolite content in medicinal herbs. *Physiologia Plantarum*, **173**(1), 321-339 (2021).

915 Pan, J. et al. Kenaf biochar enhances heavy metal phytostabilization and growth of industrial hemp
916 (Cannabis sativa L.) using multi-metal contaminated mining site soils. *Plant Physiology and*
917 *Biochemistry*, 110312 (2025).

918 Pehlivan, N., and Wang, J. J. Transcriptional insights into Cu related tolerance strategies in maize
919 linked to a novel tea-biochar. *Environmental Pollution*, **293**, 118500 (2022).

920 Peng, H., and Guo, J. Removal of chromium from wastewater by membrane filtration, chemical
921 precipitation, ion exchange, adsorption electrocoagulation, electrochemical reduction,
922 electrodialysis, electrodeionization, photocatalysis and nanotechnology: a review. *Environmental*
923 *chemistry letters*, **18**(6), 2055-2068 (2020).

924 Phares, C. A. et al. Application of biochar and inorganic phosphorus fertilizer influenced
925 rhizosphere soil characteristics, nodule formation and phytoconstituents of cowpea grown on
926 tropical soil. *Heliyon*, **6**(10) (2020).

927 Pourakbar, L., Khayami, M., Khara, J., and Farbodnia, T. Copper-induce change in antioxidative
928 system in maize (Zea mays L.). *Pakistan Journal of Biological Sciences*, **10**(20), 3662-3667
929 (2007).

930 Qamer, Z. et al. Review of oxidative stress and antioxidative defense mechanisms in Gossypium
931 hirsutum L. in response to extreme abiotic conditions. *Journal of Cotton Research*, **4**(1), 9 (2021).

932 Qayyum, M. F. et al. Effects of various biochars on seed germination and carbon mineralization
933 in an alkaline soil. *Pakistan Journal of Agricultural Sciences*, **51**, 977-982 (2015).

934 Quartacci, M. F., Sgherri, C., and Frisenda, S. Biochar amendment affects phenolic composition
935 and antioxidant capacity restoring the nutraceutical value of lettuce grown in a copper-
936 contaminated soil. *Scientia Horticulturae*, **215**, 9-14 (2017).

937 Rajendran, M. et al. Chromium detoxification mechanism induced growth and antioxidant
938 responses in vetiver (Chrysopogon zizanioides (L.) Roberty). *Journal of Central South*
939 *University*, **26**(2), 489-500 (2019).

Ramzan, M. et al. Modulation of sunflower growth via regulation of antioxidants, oil content and gas exchange by arbuscular mycorrhizal fungi and quantum dot biochar under chromium stress. *BMC Plant Biology*, **23**(1), 629 (2023).

Reif, B. M., and Murray, B. P. Chromium Toxicity. In *StatPearls [Internet]*. StatPearls Publishing. (2024).

Rizwan, M. et al. Mechanisms of biochar-mediated alleviation of toxicity of trace elements in plants: a critical review. *Environmental Science and Pollution Research*, **23**(3), 2230-2248 (2016).

Rizwan, M. et al. Residual effects of biochar on growth, photosynthesis and cadmium uptake in rice (Oryza sativa L.) under Cd stress with different water conditions. *Journal of environmental management*, **206**, 676-683 (2018).

Sahoo, S. S. et al. Production and characterization of biochar produced from slow pyrolysis of pigeon pea stalk and bamboo. *Cleaner engineering and technology*, **3**, 100101 (2021).

Sajad, M. A. et al. Evaluation of chromium phytoremediation potential of some plant species of Dir Lower, Khyber Pakhtunkhwa, Pakistan. *Acta Ecologica Sinica*, **40**(2), 158-165 (2020).

Salam, A. K. et al. The biochar-improved growth-characteristics of corn (Zea mays L.) in a 22-years old heavy-metal contaminated tropical soil. In *IOP Conference Series: Earth and Environmental Science* **1034,** 012045 IOP Publishing. (2022).

Sami, H. et al. Remediation potential of biochar and selenium for mitigating chromium-induced stress in spinach to minimize human health risk. *South African Journal of Botany*, *163*, 237-249 (2023).

Schmidt, H.et al. Permanence of soil applied biochar. *Biochar J*, 69-74. (2022).

Sehrish, A. K. et al. Effect of poultry litter biochar on chromium (Cr) bioavailability and accumulation in spinach (Spinacia oleracea) grown in Cr-polluted soil. *Arabian Journal of Geosciences*, **12**(2), 57 (2019).

Seleiman, M. F.et al. Chromium resistant microbes and melatonin reduced Cr uptake and toxicity, improved physio-biochemical traits and yield of wheat in contaminated soil. *Chemosphere*, **250**, 126239 (2020).

Shah, S. A., and Aslam, S. Nanoparticle-mediated mitigation of heavy metal stress in plants: a comprehensive review. *Journal of Nanoparticle Research*, **27**(12), 324 (2025).

Shahid, M. et al. Chromium speciation, bioavailability, uptake, toxicity and detoxification in soil-plant system: A review. *Chemosphere*, **178**, 513-533 (2017).

Shanker, A. K. Chromium: environmental pollution, health effects and mode of action. (2019).

Sharma, P. et al. Combined application of earthworms and plant growth promoting rhizobacteria improve metal uptake, photosynthetic efficiency and modulate secondary metabolites levels under chromium metal toxicity in Brassica juncea L. *Journal of Hazardous Materials*, **482**, 136489 (2025).

Siddiqui, M. M. et al. Toxic effects of heavy metals (Cd, Cr and Pb) on seed germination and growth and DPPH-scavenging activity in Brassica rapa var. turnip. *Toxicology and Industrial Health*, **30**(3), 238-249 (2014).

Singh, B., Singh, B. P., and Cowie, A. L. Characterisation and evaluation of biochars for their application as a soil amendment. *Soil Research*, **48**(7), 516-525 (2010).

Singleton, V. L., and Rossi, J. A. Colorimetry of total phenolics with phosphomolybdic-phosphotungstic acid reagents. *American journal of Enology and Viticulture*, **16**(3), 144-158 (1965).

Somboon, S. et al. Transformations in physicochemical properties and pore structure of biochar derived from rice straw revealed by synchrotron techniques. *Scientific Reports*, **15**(1), 23641 (2025).

Somboon, S. et al. Transformations in physicochemical properties and pore structure of biochar derived from rice straw revealed by synchrotron techniques. *Scientific Reports*, **15**(1), 23641 (2025).

Srivastava, D. et al. Chromium stress in plants: toxicity, tolerance and phytoremediation. *Sustainability*, **13**(9), 4629 (2021).

Su, J. et al. Mn-modified bamboo biochar improves soil quality and immobilizes heavy metals in contaminated soils. *Environmental Technology & Innovation*, **34**, 103630 (2024).

994 Tomczyk, A., Sokołowska, Z., and Boguta, P. (2020). Biochar physicochemical properties:
995 pyrolysis temperature and feedstock kind effects. *Reviews in Environmental Science and*
996 *Bio/Technology*, *19*(1), 191-215.

997 Trevelyan, W. E., and Harrison, J. Studies on yeast metabolism. 5. The trehalose content of baker's
998 yeast during anaerobic fermentation. *Biochemical Journal*, **62**(2), 177 (1956).

999 Turan, V. et al. Promoting the productivity and quality of brinjal aligned with heavy metals
1000 immobilization in a wastewater irrigated heavy metal polluted soil with biochar and
1001 chitosan. *Ecotoxicology and environmental safety*, **161**, 409-419 (2018).

1002 Vallverdú-Queralt, A. et al. A comprehensive study on the phenolic profile of widely used culinary
1003 herbs and spices: Rosemary, thyme, oregano, cinnamon, cumin and bay. *Food chemistry*, **154**,
1004 299-307 (2014).

1005 Wakeel, A., Xu, M., and Gan, Y. Chromium-induced reactive oxygen species accumulation by
1006 altering the enzymatic antioxidant system and associated cytotoxic, genotoxic, ultrastructural, and
1007 photosynthetic changes in plants. *International journal of molecular sciences*, **21**(3), 728 (2020).

1008 Wang, J. et al. Analysis of the long-term effectiveness of biochar immobilization remediation on
1009 heavy metal contaminated soil and the potential environmental factors weakening the remediation
1010 effect: A review. *Ecotoxicology and Environmental Safety*, **207**, 111261 (2021).

1011 Wei, J. et al. Assessing the effect of pyrolysis temperature on the molecular properties and copper
1012 sorption capacity of a halophyte biochar. *Environmental Pollution*, **251**, 56-65 (2019).

1013 Wolf, N. et al. Dry matter analysis methods. A report to the Manure Testing Manual Joint
1014 Committee NCR-13. SERA-6/NEC-67 (1997).

1015 Wu, P. et al. Time-dependent evolution of Zn (II) fractions in soils remediated by wheat straw
1016 biochar. *Science of the Total Environment*, **717**, 137021 (2020).

1017 Xu, X. et al. Biochar as both electron donor and electron shuttle for the reduction transformation
1018 of Cr (VI) during its sorption. *Environmental pollution*, **244**, 423-430 (2019).

1019 Yang, J. et al. Toxicity of vanadium in soil on soybean at different growth stages. *Environmental*
1020 *Pollution*, **231**, 48-58 (2017).

Yang, L. et al. Biochar improves sugarcane seedling root and soil properties under a pot experiment. *Sugar technology*, **17**(1), 36-40 (2015).

Younis, U. et al. Biochemical characterization of cotton stalks biochar suggests its role in soil as amendment and decontamination. *Advances in Environmental Research*, *6*(2), 127-137 (2017).

Younis, U. et al. Sustainable remediation of chromium-contaminated soils: boosting radish growth with deashed biochar and strigolactone. *BMC Plant Biology*, **24**(1), 115 (2024).

Yu, H. et al. Characteristics of tar formation during cellulose, hemicellulose and lignin gasification. *Fuel*, **118**, 250-256 (2014).

Yuan, C. et al. A meta-analysis of heavy metal bioavailability response to biochar aging: Importance of soil and biochar properties. *Science of the Total Environment*, **756**, 144058 (2021).

Zahra, A. et al. Wood biochar induced metal tolerance in Maize (Zea mays L.) plants under heavy metal stress. *Environmental Research*, *262*, 119940 (2024).

Zhang, J. et al. Effects of pH, dissolved humic acid and Cu^{2+} on the adsorption of norfloxacin on montmorillonite-biochar composite derived from wheat straw. *Biochemical Engineering Journal*, **130**, 104-112 (2018).

Zhang, K. et al. Photochemistry of biochar during ageing process: Reactive oxygen species generation and benzoic acid degradation. *Science of the Total Environment*, **765**, 144630 (2021).

Zhang, Z. et al. Preparation and characterization of apricot kernel shell biochar and its adsorption mechanism for atrazine. *Sustainability*, **14**(7), 4082 (2022).

Zhu, H. et al. Efficient removal of Pb^{2+} by Tb-MOFs: identifying the adsorption mechanism through experimental and theoretical investigations. *Environmental Science: Nano*, **6**(1), 261-272 (2019).

Zoufan, P. et al. Modification of oxidative stress through changes in some indicators related to phenolic metabolism in Malva parviflora exposed to cadmium. *Ecotoxicology and Environmental Safety*, **187**, 109811 (2020).